HHS Public Access

Author manuscript

Dev Cell. Author manuscript; available in PMC 2023 January 10.

Published in final edited form as:

Dev Cell. 2022 January 10; 57(1): 80–94.e7. doi:10.1016/j.devcel.2021.12.004.

chinmo-mutant spermatogonial stem cells cause mitotic drive by evicting non-mutant neighbors from the niche

Chen-Yuan Tseng[1], **Michael Burel**[1], **Michael Cammer**[2], **Sneh Harsh**[1], **Maria Sol Flaherty**[1], **Stefan Baumgartner**[4,5], **Erika A. Bach**[1,3,6]

[1]Department of Biochemistry and Molecular Pharmacology

[2]DART Microscopy Laboratory

[3]Helen L. and Martin S. Kimmel Center for Stem Cell Biology, NYU Grossman School of Medicine, New York, NY 10016, USA

[4]Department of Experimental Medical Sciences, Lund University, 22184 Lund, Sweden

[5]Department of Biology, University of Konstanz, 78467 Konstanz, Germany

[6]Lead contact

SUMMARY

Niches maintain a finite pool of stem cells via restricted space and short-range signals. Stem cells compete for limited niche resources, but the mechanisms regulating competition are poorly understood. Using the *Drosophila* testis model, we show that germline stem cells (GSCs) lacking the transcription factor Chinmo gain a competitive advantage for niche access. Surprisingly, *chinmo*$^{-/-}$ GSCs rely on a new mechanism of competition in which they secrete the extracellular matrix protein Perlecan to selectively evict non-mutant GSCs and then upregulate Perlecan-binding proteins to remain in the altered niche. Over time, the GSC pool can be entirely replaced with *chinmo*$^{-/-}$ cells. As a consequence, the mutant *chinmo* allele acts as a gene drive element: the majority of offspring inherit the allele despite the heterozygous genotype of the parent. Our results suggest the influence of GSC competition may extend beyond individual stem cell niche dynamics to population-level allelic drift and evolution.

Graphical Abstract

Correspondence: erika.bach@nyu.edu.

AUTHOR CONTRIBUTIONS

Conceptualization, MSF, MB, CYT, EAB; Investigation, CYT, MB, MSF, MC, SH, SB; Supplied Key Reagents, SB; Manuscript Writing, CYT, MB, EAB; Funding, CYT, MB, EAB; Supervision, EAB

DECLARATION OF INTERESTS

The authors declare no interests.

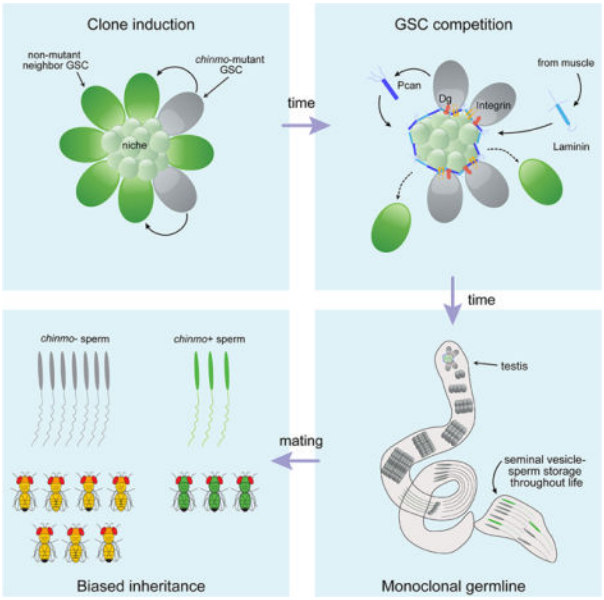

eTOC Blurb

How stem cells compete for niche access remains largely unknown. Tseng et al. show that spermatogonial stem cells (SSCs) lacking the transcription factor Chinmo remodel the niche to their own benefit, causing the expulsion of non-mutant SSCs. This leads to a homozygous germline and biased inheritance of the *chinmo*-mutant allele.

Keywords

Drosophila ; testis; germline stem cell; niche; competition; chinmo; Perlecan; Laminin; Dystroglycan; biased inheritance; aging

INTRODUCTION

Stem cells reside in discrete microenvironments called niches that maintain a supply of undifferentiated stem cells via molecular signals. Because these signals are short-range and niche space is often limited, stem cells compete with one another for niche occupancy. In stem cell competition, “winners” remain in the niche and retain stem cell identity while “losers” exit and differentiate (Simons and Clevers, 2011). Under normal conditions, stem cells compete through a stochastic process: any given stem cell has an equal probability of remaining in the niche or being lost and replaced by its neighbor. In this homeostatic process, known as neutral competition, no one stem cell has a long-term competitive advantage over another (Klein and Simons, 2011). Competition can be biased if one stem cell gains an advantage over the others. Indeed, one advantaged stem cell and its progeny can hijack a niche to compose the entire stem cell pool, resulting in tissue monoclonality (Vermeulen et al., 2013, Amoyel et al., 2014, Issigonis et al., 2009, Snippert et al., 2014). However, the factors and mechanisms regulating stem cell competition – and germline stem cell competition in particular - remain largely mysterious.

The *Drosophila* testis is an ideal model system to study stem cell competition due to its well-characterized niche, genetic tractability, and conserved stem cell maintenance pathways (Fig. 1A and (Greenspan et al., 2015)). The testis is a coiled blind-ended tube, enveloped by a muscle sheath, responsible for spermatogenesis throughout adult male life (Hardy et al., 1979, Fuller, 1998). The niche includes a group of post-mitotic cells, which is anchored to the testis apex by integrins (Tanentzapf et al., 2007). The niche secretes self-renewal signals that support two distinct stem cell populations. GSCs divide continuously throughout life and ultimately produce sperm. Approximately 8 GSCs adhere to the niche through the adhesion molecule E-Cadherin (E-Cad) (Yamashita et al., 2003). The niche also supports somatic cyst stem cells (CySCs), which co-differentiate with GSCs into post-mitotic cysts that enclose developing spermatogonia (Hardy et al., 1979, Fabrizio et al., 2003).

Stem cells in the *Drosophila* testis, as those in other tissues and organisms, compete for limited niche space and resources. CySCs have documented competitive behavior, and several mechanisms triggering biased competition in favor of single CySCs have been uncovered (Amoyel et al., 2016, Amoyel et al., 2014, Issigonis et al., 2009, Singh et al., 2010, Stine et al., 2014). Significantly less is known, however, about competition in GSCs. Regular GSC loss and replacement by neighbors has been observed (Wallenfang et al., 2006, Sheng and Matunis, 2011, Salzmann et al., 2013). While this behavior is suggestive of neutral competition, no underlying mechanisms have been elucidated. Biased competition has also never been observed in male GSCs, though single female GSCs harboring specific genetic mutations can outcompete their neighbors in the *Drosophila* ovary (Jin et al., 2008, Rhiner et al., 2009).

Here we report biased competition in male GSCs driven by mutations in the transcriptional repressor Chinmo (Zhu et al., 2006). Chinmo is a known regulator of somatic stem cell activity in the *Drosophila* ventral nerve cord and testis (Flaherty et al., 2010, Narbonne-Reveau et al., 2016). In the testis, Chinmo is required for the maintenance of male sexual identity. CySCs devoid of Chinmo undergo sex-reversal and transdifferentiate into feminized somatic stem cells (Grmai et al., 2018, Ma et al., 2014, Ma et al., 2016). Despite transcriptomic analyses of somatic stem cells lacking Chinmo, direct Chinmo target genes have not yet been identified (Grmai et al., 2021, Narbonne-Reveau et al., 2016). Here, we show that loss of *chinmo* in single GSCs confers a competitive advantage for niche access so that, over time, the GSC pool becomes “fixed” with $chinmo^{-/-}$ cells. Surprisingly, $chinmo^{-/-}$ GSCs do not rely on increased proliferation or canonical adhesion systems to gain their advantage. Instead, $chinmo^{-/-}$ GSCs ectopically secrete the extracellular matrix protein (ECM) Perlecan (Pcan) that creates a de novo ECM around the niche within the testis lumen. This resculpted niche selectively evicts non-mutant GSCs from the niche but retains $chinmo^{-/-}$ GSCs, which upregulate ECM-binding proteins. As a result this competition, the majority of adult offspring inherit the mutant *chinmo* allele despite the heterozygous genotype of the parent. These results provide the experimental evidence that GSC competition underlie “mitotic” drive, a proposed but not proven mechanism by which GSCs with a competition advantage transmit greater than the expected 50% Mendelian ratio (Otto and Hastings, 1998). Thus, GSC competition may not only be important for understanding the fundamental principles of stem cell dynamics but also have long-term implications for genetic drift and evolution (Hastings, 1989).

RESULTS

chinmo$^{-/-}$ GSCs evict non-mutant neighbor GSCs from the niche

Chinmo is expressed in male GSCs (Fig. S1A), but its role in these cells is unknown. To investigate this, we used mitotic recombination to induce single GFP-negative control and *chinmo* homozygous mutant (*chinmo*$^{-/-}$) clones in adult flies and monitored their niche retention and lineages over time (Fig. 1B). We used a null allele (*chinmo*^{1}), a hypomorphic allele (*chinmo*^{k13009}) and validated RNAi-depletion (*chinmo-i*) to generate *chinmo*-deficient GSCs clones (Fig. S1A–F). Control GSC clones and *chinmo*-deficient GSC clones were induced at the same frequency as assessed at 2 days post clone induction (dpci) (Fig. 1C,D). Both types of clones contained single, Vasa-positive cells at the niche that had dot fusomes characteristic of GSCs (Fig. 1G,H). Surprisingly, *chinmo*$^{-/-}$ GSCs composed a majority of the GSC pool by 28 dpci (Fig. 1F) compared to control clones (Fig. 1E). Prior work has shown that mutant CySCs with a competitive advantage prevail over both wild-type (WT) CySCs and WT GSCs for niche access. In contrast, *chinmo*$^{-/-}$ GSCs only outcompeted non-mutant GSCs while leaving the CySC population unaffected. We observed comparable numbers of CySCs expressing the stem cell marker Zfh1 in testes harboring either *chinmo*$^{-/-}$ or control GSC clones (Fig. 1-I, Table S1 **#16**). Thus, *chinmo*$^{-/-}$ GSCs provide a new model system for studying GSC-GSC specific stem cell competition.

We hypothesized that single GSCs lacking *chinmo* gain a competitive advantage over their non-mutant neighbors for niche access, so we quantified the percent of clones composing the GSC pool, which we termed “clone occupancy,” at 2, 7, 14, 21, and 28 dpci (Fig. 1B). At 2 dpci, both control and *chinmo*$^{-/-}$ GSC clones occupied the niche in equal proportions (Fig. 1M, Table S1 **#37–46**). By 28 dpci, however, *chinmo*$^{-/-}$ GSCs occupied a majority of the GSC pool (78.52 ± 3.77%, Table S1 **#16**), while control clones occupied significantly less (45.97 ± 5.00%, $P < 2 \times 10^{-5}$, Table S1 **#11**) (Fig. 1J). *chinmo*$^{-/-}$ GSCs occupied a majority of the GSC pool at 7, 14, and 21 dpci (Fig. 1J, Table S1 **#13–15**). Similar trends were observed at 14 dpci for the other *chinmo* alleles (Table S1 **#76,80**). Indeed, the probability of recovering testes with “fixed” niches - where a GSC clone composed the entire GSC pool - was significantly higher when GSC clones lacked *chinmo* (12.50% vs. 54.00% in control and *chinmo*$^{-/-}$ clones, respectively, at 28 dpci, $P < 3 \times 10^{-7}$) (Fig. 1K, Table S1 **#17–26**). These data indicate that loss of *chinmo* in single GSCs biases competition for niche access in their favor.

To determine whether *chinmo*$^{-/-}$ GSC clones expanded their niche presence by over-proliferation and/or by losing non-mutant neighbor GSCs, we quantified the average number of GSC clones and the average number of non-mutant neighbor GSCs over time in testes containing either control or *chinmo*$^{-/-}$ clones. Control and *chinmo*$^{-/-}$ clones themselves were present at nearly identical levels over time (3.68 ± 0.45 vs. 3.46 ± 0.25, control and *chinmo*$^{-/-}$ clones, respectively, by 28 dpci, P = 0.47) (Fig. 1M, Table S1 **#37–46**). By contrast, neighbor GSCs were precipitously lost from the niche in the presence of *chinmo*$^{-/-}$ but not control clones (4.38 ± 0.46 vs. 1.00 ± 0.18 neighbors of control or *chinmo*$^{-/-}$ clones, respectively, by 28 dpci, $P = 7 \times 10^{-7}$) (Fig. 1N, Table S1 **# 47–56**). As a result, niches harboring *chinmo*$^{-/-}$ clones experienced a net loss in total GSCs (8.05 ± 0.29 vs. 4.46 ± 0.22

in control and *chinmo*$^{-/-}$ clones, respectively, at 28 dpci, P = 4 × 10^{-21}) (Fig. 1L, Table S1**, #27–36**). We obtained similar results with other *chinmo* alleles (Table S1**, #98,102**). These results suggest that *chinmo*$^{-/-}$ GSCs gain their competitive advantage not by increasing their numbers but rather by imperiling niche access of neighbor GSCs (Fig. 1O).

chinmo$^{-/-}$ GSCs ectopically secrete Pcan into the niche milieu

The competitive advantages of *chinmo*$^{-/-}$ GSCs could result from behaviors observed in "winning" cells in the *Drosophila* ovary or epithelia, including increased proliferation, increased E-Cad, or induced death of neighbors (Jin et al., 2008, Amoyel and Bach, 2014). However, there were no substantial differences in these parameters between *chinmo*$^{-/-}$ GSC clones and control GSC clones or non-mutant neighbors (Fig. S2A–C). Additionally, *chinmo*$^{-/-}$ GSC clones still divided asymmetrically as evidenced by the mother centrosome being located at the GSC-niche interface and the daughter centrosome 180° away (Fig. S2D–F). We considered the possibility that *chinmo*$^{-/-}$ GSCs had increased self-renewal signaling compared to neighbors. GSCs require BMP/Mad and JAK/STAT pathways for self-renewal and niche adhesion, respectively (Leatherman and Dinardo, 2010). However, there are no differences in phosphoMad or phospho-STAT between *chinmo*$^{-/-}$ clones and their non-mutant neighbors (Fig. S2G–H). We observed similar robust E-Cad levels at the GSC-niche interface in *chinmo*$^{-/-}$ clones and in their non-mutant neighbor GSCs (Fig. S2I), suggesting decreased E-Cad levels were not responsible for neighbor loss.

Electron micrograph of the stem cell niche at 28 dpci revealed a ring of proteinaceous material encircling the niche in testes with *chinmo*$^{-/-}$ GSCs but not those with control GSC clones (Fig. 2A,B). This material resembled and was contiguous with the ECM composing the muscle basal lamina (BL). We termed this structure the "moat" because it resembled the ditch around a castle. A similar "gap" between GSCs and the niche can be observed at 28 dpci in single confocal images of testes with *chinmo*$^{-/-}$ GSC clones (Fig. S3B) but not with control GSC clones (Fig. S3A). The majority of *chinmo*$^{-/-}$ GSCs were displaced significantly farther from the niche by 28 dpci than control clones (Fig. S3C, compare blue to gray bar). Moats were observed in a majority of testes with *chinmo*$^{-/-}$ clones but only rarely seen in testes with control clones (Fig. S3D). Based on these results, we speculate that *chinmo*$^{-/-}$ GSCs secrete ectopic ECM into the niche milieu.

We examined expression of Pcan, a conserved secreted proteoglycan that cross-links the ECM, allows for cell-ECM adhesion, and facilities ligand diffusion (Broadie et al., 2011). In testes with control GSC clones, Pcan is found in the muscle BL and not within the testis lumen at 21 dpci (Fig. 2C,G). However, Pcan localized to the moat when *chinmo*$^{-/-}$ GSCs were present and this was observed as early as 7 dpci (Fig. 2D,G, Fig. S3E,F). We also examined expression of Laminin (Lan), a major component of BL. In testes with control GSC clones, Lan localized to the muscle BL and not the testis lumen (Fig. 2E,G). However, Lan localized to the moat when *chinmo*$^{-/-}$ GSCs were present as early as 7 dpci (Fig. 2F,G, Fig. S3G,H). Further, 3D reconstructions of confocal z-stacks revealed that Lan surrounded the niche in testes with *chinmo*$^{-/-}$ clones but not those with control clones (Fig. 3H,I, Movie S1). Other ECM proteins were expressed at low levels in testes and were not localized to the moat (Fig. S3M–T), indicating that the moat is specifically composed of Pcan and Lan.

Pcan is necessary and sufficient for perturbing neighbor GSC niche occupancy

If ectopic Pcan underlies the competitive advantage of *chinmo*$^{-/-}$ GSCs, these should be true: (1) Lan accumulation in the moat should depend on Pcan secretion by *chinmo*$^{-/-}$ GSCs; (2) ectopic Pcan secretion should be sufficient to induce GSC loss in an otherwise WT testis; and (3) *chinmo*$^{-/-}$ GSCs should require Pcan for their competitive properties.

To test the first condition, we generated positive-marked *chinmo*$^{-/-}$ GSC clones and *chinmo*$^{-/-}$ GSC clones depleted for Pcan. In testes with *chinmo*$^{-/-}$ GSC clones, Pcan is found in the moat (Fig. 2J,N) but this was significantly reduced when these clones were depleted for Pcan (Fig. 2K,N). Lan in the moat also declined significantly in *chinmo*$^{-/-}$ clones depleted for Pcan (Fig. 2L,M,O). These results indicate that the moat is caused by ectopic Pcan secretion by *chinmo*$^{-/-}$ GSCs and suggest that Lan is recruited to the moat from the muscle BL. In support of this, Lan in the moat was significantly reduced when Lan was depleted from muscle (Fig. S3IK). HCR-FISH revealed that *Pcan* transcripts were significantly increased in *chinmo*$^{-/-}$ GSCs compared to control GSCs (Fig. S4A–F), suggesting that *Pcan* is Chinmo target in GSCs.

To test the second condition - whether ectopic Pcan can impede WT GSCs - we used the GSC driver *nanos* (*nos*) to mis-express Pcan in otherwise WT GSCs. We observed ectopic Pcan and Lan surrounding the niche in *nos>Pcan* testes, similar to the *chinmo*$^{-/-}$ GSC phenotype (Fig. 3A–D). As expected, GSC-secreted Pcan phenocopied the loss in total GSC number (Fig. 3E, Table S1 **#57,58**) observed in testes containing *chinmo*$^{-/-}$ GSC clones at same time point (i.e., 21 days) (Fig. 1L). Thus, ectopic Pcan secreted by GSCs is sufficient to alter the niche architecture and disadvantage WT GSC niche access.

To test the third condition - whether Pcan is necessary for *chinmo*$^{-/-}$ GSCs to expel non-mutant neighbor GSCs - we used the MARCM technique to deplete Pcan using two validated RNAi lines (Fig. S1K–N) in control or *chinmo*$^{-/-}$ GSC clones. Depletion of Pcan from *chinmo*$^{-/-}$ GSC clones robustly blocked the increase in *chinmo*$^{-/-}$ clone occupancy (48.21 ± 3.49% vs. 33.52 ± 2.50% in *chinmo*$^{-/-}$ and *chinmo*$^{-/-}$, *Pcan*-RNAi clones, respectively, at 14 dpci, $P < 0.0018$) (Fig. 3F, Table S1 **#68, 70**). By contrast, clone occupancy of control clones was unaffected by Pcan depletion (Fig. 3F, Table S1 **#60, 62**). This reduction in competitive behavior is not because Pcan-depleted *chinmo*$^{-/-}$ GSCs were lost from the niche (Fig. 3I, Table S1 **#134, 136**), but rather because non-mutant neighbor GSCs were no longer preferentially evicted (3.37 ± 0.27 vs. 4.67 ± 0.23 WT neighbors of *chinmo*$^{-/-}$ and *chinmo*$^{-/-}$, *Pcan*-RNAi clones, respectively, at 14 dpci, $P < 0.0006$) (Fig. 3H, Table S1**, #112, 114**). Consistent with the partial rescue of neighbor GSCs, the average total number of GSCs was also significantly increased by depleting Pcan in *chinmo*$^{-/-}$ GSCs (6.28 ± 0.26 vs. 6.97 ± 0.19 GSCs in testes with *chinmo*$^{-/-}$ and *chinmo*$^{-/-}$, Pcan-RNAi clones, respectively, at 14 dpci, $P < 0.044$) (Fig. 3G, Table S1 **#90, 92**). A similar autonomous requirement for Pcan was observed in *chinmo*^{k13009} clones (Table S1, **#76, 78, 98, 100, 120, 122)**. By contrast, Lan depletion from *chinmo*$^{-/-}$ GSC clones using a validated RNAi line (Fig. S1H–J) did not significantly alter clone occupancy, the average number of GSCs, or the average number of neighbors (Table S1 **#74, 96, 118**). Thus, removal of Pcan but not Lan from *chinmo*$^{-/-}$ GSCs greatly impairs their competitive phenotype. Consistent

with the model that Lan is recruited to the moat, depleting Lan from the muscle significantly reduced Lan in the moat and the clone occupancy of *chinmo*$^{-/-}$ GSCs (Fig. S3K,L, Table S1 **#147, 148**). We conclude that *chinmo*$^{-/-}$ GSCs non-autonomously compromise neighbor GSC access by secreting Pcan into the niche (Fig. 3J).

chinmo$^{-/-}$ GSCs remain in the altered niche by upregulating Dystroglycan (Dg)

We reasoned that *chinmo*$^{-/-}$ GSCs remain in the niche because they upregulate ECM-binding proteins. Dg is a transmembrane protein that interacts with Pcan via its extracellular domain and the actin cytoskeleton via its intercellular domain (Schneider et al., 2006). Dg is significantly increased at the GSC-niche interface in *chinmo*$^{-/-}$ GSCs but not in control GSC clones (Fig. 4A–C). Furthermore, HCR-FISH revealed that *Dg* transcripts were significantly increased in *chinmo*$^{-/-}$ GSCs compared to control GSCs (Fig. S4G–I), suggesting that *Dg* may be regulated by Chinmo in GSCs. To test this, we depleted Dg using a validated RNAi line (Fig. S1O–Q) from control and *chinmo*$^{-/-}$ clones. Depleting Dg from *chinmo*$^{-/-}$ clones significantly decreased their clone occupancy (Fig. 4D, Table S1 **#154, 156**), restored the average total number of GSCs (Fig. 4E, Table S1 **#166, 168**) and rescued non-mutant neighbors (Fig. 4F, Table S1 **#178, 180**). Dg knockdown in *chinmo*$^{-/-}$ clones – but not control clones - caused a slight but significant decrease in clone recovery at 14 dpci (Fig. 4G, Table S1 **#190, 192**). Similar results were observed with the *chinmo*^{k13009} allele (Table S1 **#158, 160, 170, 172, 182, 184, 194, 196)**. We conclude that Dg expression is an important mechanism used by *chinmo*$^{-/-}$ GSCs to remain in the remodeled niche (Fig. 4H).

chinmo$^{-/-}$ GSCs remain in the altered niche via βPS integrin

We next examined integrins, which mediate cell-ECM interactions, in GSC competition. The integrin-associated protein Talin is significantly increased at the GSC-niche interface in *chinmo*$^{-/-}$ GSC clones compared to non-mutant GSC neighbors (Fig. S5B,C). By contrast, there is no significant change in Talin levels between control GSC clones compared to their neighbor GSCs (Fig. S5A,C). Only βPS - and not other integrin subunits - was increased at the GSC-niche interface in *chinmo*-deficient GSCs (Fig. S5D–P). HCR-FISH revealed that *βPS* transcripts were significantly increased in *chinmo*-depleted GSCs compared to control GSCs (Fig. S4J–L), suggesting that *βPS* may be regulated by Chinmo in GSCs.

To determine whether Talin or βPS was required for *chinmo*$^{-/-}$ clones to remain in the altered niche, we depleted either factor using validated RNAi lines (Fig. S1R–Y) in control or *chinmo*$^{-/-}$ clones and assessed parameters of competition. Knocking down Talin in *chinmo*$^{-/-}$ clones significantly decreased their clone occupancy (Fig. S6A, Table S1 **#202, 204**), restored the average total number of GSCs (Fig. S6B, Table S1 **#210, 212**) and rescued non-mutant neighbors (Fig. S6C, Table S1 **#218, 220**). Talin depletion from *chinmo*$^{-/-}$ clones - but not from control clones - reduced their niche residence (Fig. S6D, Table S1 **#226, 228**). Depleting βPS with either RNAi line in *chinmo*$^{-/-}$ clones significantly decreased clone occupancy (Fig. S6E, Table S1 **#236, 238, 240**), restored the average total number of GSCs (Fig. S6F, Table S1 **#248, 250, 252**) and rescued non-mutant neighbors (Fig. S6G, Table S1 **#260, 262, 264**). Control GSC clones depleted for βPS using RNA-i #1 could not be recovered at 2 dcpi (Fig. S6H, Table S1 **#267**), and control clone recovery was greatly reduced using the second βPS RNAi line (Table S1 **#269**). These data suggest

that βPS is required for GSC maintenance. We could not test this hypothesis using mosaic analysis because mutation of the X-linked *βPS* gene is male lethal. However, in support of this model, there were significantly fewer GSCs at the niche when βPS or Talin were depleted from GSCs (Fig. S1Z). Importantly, *chinmo*$^{-/-}$ GSC clones depleted for βPS could remain in the altered niche (Fig. S6H, Table S1 **#273, 274**). These results indicate that increased integrin expression is used by *chinmo*$^{-/-}$ GSCs to remain in the resculpted niche (Fig. S6I). They also demonstrate that Dg and βPS integrin are non-redundant mechanisms employed by competitive GSCs for niche occupancy. Downregulation of ECM binding proteins in the *chinmo*$^{-/-}$ clone alters Pcan and Lan levels in the moat. In testes with *chinmo*$^{-/-}$ GSCs depleted for βPS or Dg, there is significantly less Pcan and Lan in the moat (Fig. 2N,O). These results suggest that (1) there is a feedback loop from ECM binding receptors promoting Pcan secretion or (2) ECM binding proteins in GSCs stabilize the moat.

Providing neighbors with more Dg rescues them from competition

We next tested whether non-mutant neighbor GSCs supplied with more Dg would adhere to the moat and be rescued from competition (Fig. 5A). To test this, we mis-expressed Dg in all GSCs using *nos* and then generated control or *chinmo*$^{-/-}$ GSC clones. We compared the number of non-mutant neighbor GSCs at 14 dpci when competition is robustly occurring (Fig. 5B). The moat generated by *chinmo*$^{-/-}$ GSCs (Fig. 5C,F) was still observed when Dg was mis-expressed in all GSCs (Fig. 5D–F). Despite the presence of the moat, non-mutant neighbor GSCs remained in the altered niche when they had increased Dg (Fig. 5D, yellow arrowheads, Fig. 5G, last bar, Table S2 **#6, 8**). Furthermore, the number of GSCs/testis is rescued when neighbors have increased Dg (Fig. 5H, Table S2 **#14, 16**).

GSC competition causes biased inheritance

Since testes with *chinmo*$^{-/-}$ GSCs frequently have a homozygous mutant germline, the *chinmo*$^{-/-}$ allele should be inherited at a super-Mendelian frequency (i.e., greater > 50%). To assess this, we generated males which had a *chinmo*$^{+}$ or *chinmo*$^{-}$ allele *in trans* to a *ubi-GFP*-labeled sister chromosome that could be scored in the next generation (Fig. 6A). We generated *chinmo*$^{+/+}$ GSC clones or *chinmo*$^{-/-}$ GSC clones and aged the males until 21 dpci, at which time we mated single males with two virgin WT females for two days. At 23 dpci, we isolated the testes of the mated males and assessed germline clonality. Our model predicts that if competitive *chinmo*$^{-/-}$ GSCs cause mitotic drive, the *chinmo*$^{-}$ chromosome should be inherited by more than 50% of the F1 progeny while the GFP-positive sister chromosome should be passed on to less than 50%. By contrast, since *chinmo*$^{+/+}$ GSCs should not have a competitive advantage, the *chinmo*$^{+}$ chromosome should be inherited by 50% of the F1 progeny and the GFP-positive sister chromosome should be inherited by the other 50% (Fig. 6A).

As expected, testes with *chinmo*$^{+/+}$ clones contained both GFP-negative GSC clones and GFP-positive non-mutant neighbor GSCs (Fig. 6B). As predicted, testes with *chinmo*$^{-/-}$ GSC clones were frequently monoclonal or “fixed”, containing only GFP-negative *chinmo*$^{-/-}$ GSCs (Fig. 6C). For the allele inheritance assay, we followed the sister chromosome by inheritance of the GFP-positive transgene it harbors (Fig. 6D, green part of each bar) and the *chinmo* allele (either *chinmo*$^{+}$ or *chinmo*$^{-}$) by inheritance of the

GFP-negative chromosome (Fig. 6D, black part of each bar). As predicted, 50% of the offspring of males with *chinmo*$^{+/+}$ GSC clones inherited the *chinmo*$^{+}$ allele and the other 50% inherited the GFP-positive sister chromosome (Fig. 6D, first bar, Table S3 **#1, 2**). Consistent with our model, 65% of offspring of males with *chinmo*^{1}-mutant GSCs clones inherited the *chinmo*^{1} mutant allele and 35% inherited the GFP-positive sister chromosome (Fig. 6D, second bar, Table S3 **#3, 4**). We see a similar trend of biased inheritance with the *chinmo*^{k13009} allele, (Fig. 6D, last bar, Table S3 **#5, 6**). These results indicate that GSC competition can cause biased inheritance.

Declining Chinmo levels in GSCs cause physiological aging of the testis niche

To assess whether the competition phenotypes could also be observed in physiological processes like aging and whether they also depended on reduced Chinmo expression, we examined testes from 2- ("young") and 42-day-old ("aged") males. Chinmo protein is expressed at a moderate level in GSCs in young testes (Fig. 7A,C) but is significantly decreased in GSCs in aged testes (Fig. 7B,C). A time course revealed that Chinmo is progressively and significantly decreased in GSCs during adulthood (Fig. 7C). The average total number of GSCs significantly declines during adulthood, and by 42 days there are on average 6.3 GSCs (Fig. 7D, Table S1 **#283**). This is similar to the decline in average total number of GSCs when *chinmo*$^{-/-}$ clones are induced in young males (Fig. 1L). A moat composed of Pcan and Lan is present in the lumen of aged but not young testes (Fig. 7E–K). Most testes from aged males had a moat, a significant increase compared to young males (Fig. 7I), that was phenotypically indistinguishable from the moat caused by competition (Fig. 2D,F). The moat is a valid age-related phenotype because it was observed two distinct genotypes, Oregon^{R} and *nos>lacZ* (see below). Additionally, GSCs in aged WT testes have increased Dg at the GSC-niche interface (Fig. 7M,N), similar to what we observe in *chinmo*$^{-/-}$ GSCs in younger males (Fig. 4B). Increased Dg was not observed in GSCs in young WT testes (Fig. 7L,N).

To determine whether these aging phenotypes could be reserved by artificially maintaining Chinmo levels in GSCs throughout adulthood, we over-expressed Chinmo using *nos* (*nos>chinmo*) (Fig. 7O). As the control, we over-expressed a neutral protein lacZ using the same promoter (*nos>lacZ*). We found that all age-related phenotypes (the moat, Dg upregulation, and reduced GSC number) were significantly suppressed by maintaining moderate levels of Chinmo in GSCs throughout adulthood (Fig. 7O–X, Table S1 **#284, 285**). These data demonstrate that aging of the *Drosophila* testis stem cell niche is regulated by declining levels of Chinmo in GSCs. They also indicate that *chinmo*$^{-/-}$ GSCs in young males coopt an aging mechanism to remodel the niche to benefit themselves and to disadvantage non-mutant neighbors.

Chinmo represses Pcan expression in somatic stem cells

To test the possibility that Chinmo represses *Pcan* in other *Drosophila* stem cells to maintain tissue homeostasis, we examined the role of *Pcan* in male-to-female sex transformation of CySCs induced by loss of Chinmo. CySCs lacking *chinmo* transdifferentiate into ovarian, epithelial cells that express Fas3 and that generate an ectopic BL composed of Pcan (Fig. S7A–C"', arrowheads, E). *chinmo*-mutant CySCs depleted for Pcan had

significantly reduced Pcan deposition in the testis lumen (Fig. S7D–E), suggesting that the *chinmo*-deficient stem cells were the source of Pcan and that Chinmo normally represses Pcan in CySCs. Depleting Pcan from *chinmo*-deficient CySCs significantly reduced Fas3 expression, indicating that sex transformation was at least partially blocked (Fig. S7E). Thus, Chinmo represses *Pcan* expression in at least two distinct stem cell populations to maintain tissue function.

DISCUSSION

This work reveals an unexpected model of GSC competition that results in biased inheritance (Fig. 6E). These results provide mechanistic demonstration of the postulated "mitotic drive" by which germline stem cells with a competition advantage transmit competitive alleles at greater than the expected 50% Mendelian ratio (Otto and Hastings, 1998). Studies in plants, yeast, flies and mice have shown that selfish genetic elements can cause gene drive through various molecular mechanisms. These include "meiotic drivers" that coopt meiotic divisions or that kill viable gametes which do not inherit the selfish element (Bravo Nunez et al., 2018). "Mitotic drive" occurs earlier in the germline lineage, at the stem cell level, and is an understudied area. Prior work in the *Drosophila* ovary has shown that dedifferentiation-defective female GSCs "win" by upregulating E-Cad at the GSC-niche interface and gradually pushing WT GSCs out of the niche (Jin et al., 2008). Since differentiation-defective GSCs do not differentiate into gametes, this study could not examine biased allele inheritance. Female GSCs with 4x gene dose of Myc were reported to be "winners" but biased inheritance was not assessed (Rhiner et al., 2009).

Given the competitive advantage of GSCs lacking *chinmo*, why has evolution not selected for male GSCs with no *chinmo* expression? Since *chinmo* is an essential gene required for development (Zhu et al., 2006), loss of *chinmo* in GSCs might cause reduced *chinmo* expression in other tissues, likely reducing organismal fitness. Furthermore, *chinmo*-dependent competition is a progressive phenotype requiring at least two weeks of adulthood. If males with mosaic *chinmo*$^{-/-}$ clones in the germline were mated as young adults, both the *chinmo*$^{+}$ and *chinmo*$^{-}$ allele would be passed on to offspring, and this would be sufficient to maintain *chinmo*$^{+}$ allele in the population. Although the GSC pool in testes with *chinmo*$^{-/-}$ cells is often monoclonal, why is the *chinmo*$^{-}$ allele is not passed on to 100% of offspring. We maintain males as virgins until we dissect their testes or until mating. This means that both *chinmo*$^{-}$ GFP-negative and *ubi-GFP*-positive spermatids are stored in the seminal vesicle throughout the male's lifetime and the single round of mating in our experiments allows for the transmission of both types of sperm.

We identified three phenotypes – competition, aging and transdifferentiation – that are dependent on ectopic *Pcan* expression in *chinmo*-deficient stem cells. This remarkable finding raises the important question of what factors regulate Chinmo expression in GSCs during adulthood and what genes are direct targets of Chinmo. We identified *chinmo* as a JAK/STAT target gene (Flaherty et al., 2010), and but STAT-deficient GSCs still express Chinmo protein (not shown), indicating that as-yet unidentified factors regulate Chinmo in GSCs and perhaps in other stem cells. Additionally, future molecular work will be needed

to determine whether *Pcan*, *Dg* and *βPS* are direct Chinmo target genes in germline and somatic stem cells.

Our work raises the possibility that other mutant stem cells can "cheat" by resculpting their microenvironment and then ensuring their own retention in this remodeled milieu. Paternal age effect disorders (PAEs) encompass a broad spectrum of spontaneous congenital disorders and are thought to arise from rare selfish GSCs have that are positively selected and clonally expand (Goriely and Wilkie, 2012). While the current model of PAE postulates increased proliferation of mutant GSCs as the competitive mechanism, other selfish cellular behaviors such of the ones we have discovered could also be functioning in the mammalian testis. Cancer stem cells could utilize the mechanisms described in our study to colonize a tissue. Leukemic stem cells induce progressive remodeling of the bone marrow niche, and this altered niche favors the mutant stem cells while impairing normal hematopoietic stem cell residence and contributes to bone marrow fibrosis (Schepers et al., 2013, Sperling et al., 2017). In sum, our work raises the possibility that selfish stem cells across species cheat using the mechanisms we have discovered in competitive GSCs in the *Drosophila* testis.

Limitations of the Study

Although our study found significant increases in *Pcan*, *Dg* and *βPS* transcripts in GSCs deficient for Chinmo, our HCR FISH analyses of relative intensity are not strictly quantitative. As such, we cannot rule out that Chinmo affects other aspects of mRNA regulation, such as splicing. Because we have as-yet not obtained the transcriptome of *chinmo*$^{-/-}$ GSCs at sufficient resolution and have not been able to perform Chinmo ChIP-seq in GSCs, we cannot conclude that Chinmo directly represses these genes. It will be important in the future to determine Chinmo occupancy on chromatin in GSCs and in other stem cells. Surprisingly, the niche spaces vacated by non-mutant neighbor GSCs are occupied by CySCs and not by *chinmo*$^{-/-}$ GSCs. We do not understand why the CySCs predominate, and future studies employing *ex vivo* live-imaging will be important to gain insights into this process.

STAR METHODS

RESOURCE AVAILABILITY

Lead contact—Further information and requests for resources and reagents should be directed to and will be fulfilled by the Lead Contact, Erika Bach (erika.bach@nyu.edu).

Materials availability—This study did not generate new unique reagents. All Drosophila stocks generated in this study are available from the Lead Contact without restriction.

Data and code availability

- All data reported in this paper will be shared by the Lead Contact upon request.
- This paper does not report original code.
- Any additional information required to reanalyze the data reported in this paper is available from the Lead Contact upon request.

EXPERIMENTAL MODEL AND SUBJECT DETAILS

Fly Lines and Maintenance—*Drosophila melanogaster* strains used in this study are listed in the Key Resources Table. *Drosophila* were reared on food made with these ingredients: 1800mL molasses (LabScientific, Catalog no. FLY-8008–16), 266 g agar (Mooragar, Catalog no. 41004), 1800 g cornmeal (LabScientific, Catalog no. FLY-8010–20), 744g Yeast (LabScientific, Catalog no. FLY-8040–20F), 47 L water, 56 g Tegosept (Sigma no. H3647–1KG), 560mL reagent alcohol (Fisher no. A962P4), and 190mL propionic acid (Fisher no. A258500). Flies were raised at 25°C except *nos-Gal4* and *mef2-Gal4* crosses, which were maintained at 18°C until eclosion, and the adult flies were transfer to 29°C.

We used the following *Drosophila* stocks: *nos-Gal4-VP16* (Van Doren et al., 1998); *tj-Gal4 (*Kyoto #104055*); UAS-lacZ* (BDSC #3956); *UAS-Pcan-i* #1 (BDSC #33642) and #2 (BDSC #29440); *Pcan-i* on II (VDRC #24549); *UAS-control-i* (BDSC #61501); *UAS-chinmo-i* (BDSC #33638); *UAS-LanB1-i* (BDSC #42616); *UAS-βPS-i* #1(BDSC #33642) and #2 (BDSC #27735); *UAS-talin-i* (BDSC #32999); *UAS-Dg-i* (BDSC #34895); *mef2-Gal4* (BDSC #50742); *UAS-Dg* (Deng et al., 2003); *βPS-GFP* (Klapholz et al., 2015); *UAS-Pcan*^{RG} (Cho et al., 2012); *chinmo*^{1} (Zhu et al., 2006); *chinmo*^{k13009}; (Kyoto #111100); *tub-Gal80*^{ts} (McGuire et al., 2004); *UAS-5'UTR-chinmo-3'UTR* (Zhu et al., 2006). For a list of full genotypes by figure, see Table S4.

We used only adult *Drosophila* males in this study.

METHODS DETAILS

***Drosophila* Genetics and Clonal Analysis—**Negatively-marked GSC clones were generated using the FLP/FRT technique after a single 1 hour heat shock at 37°C in 2-day old adult males (Xu and Rubin, 1993). Males were returned to 25°C until dissection at 2, 7, 14, 21, 23, 28 dpci.

Positively marked clones were generated by the MARCM technique after a single 1 hour heat shock at 37°C in 2-day old adult males (Lee and Luo, 1999). Males were returned to 25°C until dissection at 2, 14 dpci.

Lineage-wide mis-expression or depletion was achieved using the Gal4/UAS system (Brand and Perrimon, 1993). A *Gal80*^{ts} transgene was used with *nos-Gal4* to deplete Dg or Talin from adult GSCs in RNA-i efficiency experiments in Fig. S1O,P,T,U,W and X (McGuire et al., 2004). *tj-Gal4* was used to deplete Chinmo from CySCs for 5 days of adulthood in Fig. S7A–D.

Immunofluorescence—Dissections and staining were carried out as previously described (Flaherty et al., 2010). Briefly, testes were dissected in 1x phosphate buffered saline (PBS), fixed for 15 minutes in 4% paraformaldehyde (PFA) in 1xPBS, washed for 1 hour at 25°C in 1xPBS with 0.5% Triton X-100, and blocked in PBTB (1xPBS 0.2% Triton X-100 and 1% bovine serum albumin) for 1 hour at 25°C. Primary antibodies were incubated overnight at 4°C except for pSTAT which was incubated overnight at 25°C. They were washed two times for 30 minutes in PBTB and incubated for 2 hours in secondary antibody in PBTB at 25°C and then washed two times for 30 minute in 1xPBS with 0.2% Triton X-100.

They were mounted in Vectashield or Vectashield with DAPI (Vector Laboratories). For 5-ethynyl-20-deoxyuridine (EdU, Life Technologies) labeling, samples were incubated for 30 minutes before fixation in Ringer's medium containing 10 μM EdU. Testes were fixed and processed normally for antibody labeling and then treated per manufacturer's instructions. Confocal images were captured using Zeiss LSM 510 and LSM 700 microscopes with a 63x objective. Z-stacks for 2D and 3D images were captured on a Nikon W1 spinning disk confocal microscope with lasers at 405, 488, 561, 640 nm, narrow pass filters for emission, a SR HP Plan Apo 100X 1.35 Silicon Oil λS DIC lens, and an Andor 888 Live EMCCD camera.

Electron Microscopy—Prior to fixation, we dissected 10 testes of each genotype and visualized the extent of GFP-positivity (indicating non-mutant germ cells) under a GFP-dissecting microscope. Germ cells are the most numerous cell type in the testis, and it is relatively straightforward to gain a rough assessment of germline clonality in mosaic testes using GFP. Most of the testes with control clones contained approximately equal levels of GFP-negative and GFP-positive germ cells. Most of the testes with *chinmo*$^{-/-}$ clones contained few GFP-positive germ cells, indicating that the clones had outcompeted the non-mutant neighbors. All of the samples were processed for TEM, and we are presenting in Fig. 2A,B representative examples of each genotype.

Drosophila testes were fixed with 2.5% glutaraldehyde and 2% paraformaldehyde in 0.1 M sodium cacodylate buffer (pH 7.2) with 1 mM $CaCl_2$ for 2 hours. After fixation, they were treated with 1% osmium tetroxide for 1 hour, followed by block staining with 1% uranyl acetate aqueous solution overnight at 4°C. The samples were rinsed in water, dehydrated in graded series of ethanol, infiltrated with propylene oxide/EMbed 812 mixtures and embedded in EMbed 812 resin (Electron Microscopy Sciences, PA USA). 70 nm ultra-thin sections were cut and mounted on 200 mesh copper grids and stained with uranyl acetate and lead citrate. Imaging was performed by Talos120C transmission electron microscope (Thermo Fisher Scientific, Hillsboro, OR) and recorded using Gatan (4k × 4k) OneView Camera with software Digital Micrograph (Gatan Inc., Pleasanton, CA).

3D Image Rendering –: ImageJ 1.53 and Imaris 9.7 were used to generate 2D and 3D images in Fig. 2H,I, Fig. 7J,K and Movie S1.

Inheritance Assay—We induced control, *chinmo*^{1} or *chinmo*^{k13009} GSC clones and aged the males for 21 days. Each male was mated singly to two Oregon^{R} (WT) virgins for 2 days. At 23 dpci, we dissected the testes of each mated male to determine the germline clonality. We scored the percentage of adult F1 offspring from the mated male for the inheritance of the *chinmo*$^{+}$ allele (from control GSC clones) or the *chinmo*$^{-}$ allele (from *chinmo*^{1} or *chinmo*^{k13009} GSC clones) by the lack of GFP expression under a Zeiss Stemi 11 GFP-dissecting scope. We scored inheritance in F1 offspring of the sister chromosome, which carries a *ubi-GFP* transgene, by the expression of GFP.

Hybridization Chain Reaction (HCR) Fluorescent *in situ* Hybridization (HCR-FISH)—We purchased from Molecular Instruments, Inc. the HCR probe set against *Pcan*, *Dg* and *βPS* mRNAs, the HCR amplifier, and the hybridization, wash, and amplification

buffers. The protocol for immunostaining with HCR-FISH was adapted from (Zimmerman et al., 2013, Choi et al., 2018). Briefly, testes were fixed in 4% PFA in 0.1% Triton X-100 in 1xPBS-DEPC for 30 minutes at 25°C, washed with 0.5% Triton X-100 in 1xPBS-DEPC two times for 30 minutes at 25°C. Samples were blocked in 0.1% Triton X-100 in 1xPBS-DEPC with 50 μg/mL heparin and 250 μg/mL yeast tRNA (buffer hereafter called "PBTH"), and then they were then incubated with primary antibodies overnight at 4°C. The next day, the samples were washed twice in PBTH for 30 minutes. Samples were then incubated with fluorescently-labeled secondary antibodies in PBTH for 2 hours at 25°C. Samples were washed in PBTH twice for 30 minutes at 25°C. Samples were then dehydrated and rehydrated with a series of ethanol washes (25%, 50%, 75%, 100%) in 1xPBS-DEPC for 10 minutes at 25°C. Samples were treated for 7 minutes with 50 μg/mL Proteinase K, which was then inactivated by washing with 0.2% glycine twice in 1xPBS-DEPC for 5 minutes at 25°C. After Proteinase K treatment, the samples were fixed again in 4% PFA in 1xPBS-DEPC for 30 minutes at 25°C. The re-fixed samples were pre-hybridized in hybridization buffer provided by Molecular Instruments Inc. for 10 minutes at 25°C and then incubated with HCR probes overnight (12 – 16 hr) at 37°C. Samples were then washed 6 times 10 minutes at 37°C with wash buffer provided by Molecular Instruments Inc. and then twice for 5 min in 5xSCC at 25°C. Samples were incubated in amplification buffer provided by Molecular Instruments Inc. for 5 minutes at 25°C. The secondary reagents called "Hairpin h1 DNA" and "Hairpin h2 DNA" were prepared by heating each for 90 seconds at 95°C and cooling them at 25°C in a dark drawer for 30 minutes. Hairpin h1 DNA and Hairpin h2 DNA were mixed together at a 1:1 ratio and then added to the samples, which were then incubated in the dark environment overnight (16 hr) at 25°C. Samples were washed 6 times for 5 minutes with 5xSSC at 25°C and mounted in Vectashield plus DAPI for confocal analysis.

QUANTIFICATION AND STATISTICAL ANALYSIS

Quantification of Pcan/Lan in the moat—We captured confocal z-stacks (at 1 μM intervals) encompassing all niche cells (typically 16–20 slices) in testes with GSC clones and stained then with Pcan or Lan antibodies. The niche was counted as "with Pan/Lan" if the ECM protein was present next to at least one niche cell facing the testis lumen in any of the slices.

Quantification of βPS-GFP/Dg/Talin/E-Cad expression at the GSC-niche interface—We captured confocal z-stacks (at 1 μM intervals) encompassing all niche cells (typically 16–20 slices). We measured fluorescence intensity by ImageJ in single z slices at the area of maximal contact of a GSC with the niche. The background signal was measured in the nucleus of a gonialblast then subtracted from each GSC-niche measurement. In the mis-expression/knockdown experiments performed using the Gal4/UAS technique, each data point represents the intensity of βPS-GFP/Dg/Talin in one GSC. In the clonal analyses, the fluorescence intensity of Dg/Talin/E-Cad at the GSC-niche interface of the clone was normalized to that of a non-mutant neighbor GSC. In the clonal analyses, each data point represents one GSC.

Quantification of Chinmo protein and *Pcan*, *Dg*, *βPS* mRNAs in GSCs—We captured confocal z-stacks (at 1 μM intervals) encompassing all niche cells (typically 16–20

slices). We measured Chinmo (or HCR-probe) fluorescence intensity by ImageJ in a single z slice taken at the maximal width of the GSC. The background signal was measured in the nucleus of a muscle cell then subtracted from each measurement. Each data point represents one GSC.

Quantification of Pcan/Lan expression in the muscle basal lamina and in the testis lumen—We captured confocal z-stacks (at 1 μM intervals) encompassing the entire width of testes including the basal lamina and all niche cells (typically 20–25 slices). Measurements were performed using ImageJ on a single z section taken at the position where the niche attaches to the basal lamina. The background signal was measured in the nucleus of a niche cell then subtracted from each measurement. Each data point represents Pcan/Lan intensity in one testis.

Quantification of mis-oriented centrosomes in GSC clones—Centrosomes were labeled with a γ-tubulin antibody. GSCs with mis-oriented centrosomes were defined as having neither the mother nor the daughter centrosome located next to the niche as described in (Cheng et al., 2008). To measure the percentage of GSCs with mis-oriented centrosomes, we scanned each testis with GSC clones on a laser scanning confocal microscope. Z-sections were taken at 1 μM intervals (typically 16–20 slices in total/testis). We calculated the number of GFP-negative GSC clones and GFP-positive non-mutant neighbor GSCs with mis-oriented centrosomes (Fig. S2F).

Quantification of the GSC-niche distance—To measure the distance from GSCs to the niche (Fig. S3C), we used ImageJ to analyze images of testes captured on a laser scanning confocal microscope. We measured the distance from the GSC plasma membrane to the edge of the closest niche cell for each GSC in testes with control or *chinmo*$^{-/-}$ GSCs clones at 28 dpci.

Quantification of the number of testes with a moat—Testis with control or *chinmo*^{1} GSC clones were examined at 2, 7, 14, 21, 28 dpci for a gap (corresponding to the moat) between the GSCs and niche cells (Fig. S3D).

Statistical Analysis—Statistical analyses were performed using two-tailed Student's t-tests except in Fig. 1K, which was performed using two-way Anova, and in Figs. 2G, 2N, 2O, 5F, 6D, 7I, S2F, S3K, and S7E, which were performed using χ^2 tests; and Fig. S3D, which was performed by a Mann-Whitney test. Data were analyzed by GraphPad Prism and Microsoft Excel. Statistical significance was assumed by $P < 0.05$. Individual P values are indicated. Data are represented by the mean and standard error of mean (SEM), except Fig. S3D in which data are represented by the mean and standard deviation (SD).

Supplementary Material

Refer to Web version on PubMed Central for supplementary material.

ACKNOWLEDGEMENTS

We thank NYU Langone Health DART Microscopy Laboratory, A. Liang, C. Petzold and K. Dancel-Manning for consultation and assistance with TEM work. The Microscopy Laboratory is partially supported by Laura and Isaac Perlmutter Cancer Center Support Grant NIH/NCI P30CA016087. We thank K. White, D. Godt, P. Rangan, N. Sokol, T. Volk, G. Morata, E. Laufer, B. Hudson, M. Ringuette, S. Hayashi, M. Crozatier, Y. Nakanishi for antibodies, and T. Lee, A. Kolodkin, N. Brown, Bloomington Stock Center (BDSC) and Kyoto Stock Center for fly stocks. The BDSC is supported by a grant from the Office of the Director of the NIH (P40OD018537). We are grateful to FlyBase, which is supported by a grant from the National Human Genome Research Institute at NIH (U41 HG000739).

Work is the Bach lab is supported by grants from the NIH (R03-HD090422; R01-GM085075). CYT was supported by a New York State Department of Health/NYSTEM institutional training grant (#C322560GG).

REFERENCES

AMOYEL M, ANDERSON J, SUISSE A, GLASNER J & BACH EA 2016. Socs36E Controls Niche Competition by Repressing MAPK Signaling in the Drosophila Testis. PLoS Genet, 12, e1005815. [PubMed: 26807580]

AMOYEL M & BACH EA 2014. Cell competition: how to eliminate your neighbours. Development, 141, 988–1000. [PubMed: 24550108]

AMOYEL M, SIMONS BD & BACH EA 2014. Neutral competition of stem cells is skewed by proliferative changes downstream of Hh and Hpo. EMBO J, 33, 2295–313. [PubMed: 25092766]

BRAND AH & PERRIMON N 1993. Targeted gene expression as a means of altering cell fates and generating dominant phenotypes. Development, 118, 401–15. [PubMed: 8223268]

BRAVO NUNEZ MA, NUCKOLLS NL & ZANDERS SE 2018. Genetic Villains: Killer Meiotic Drivers. Trends Genet, 34, 424–433. [PubMed: 29499907]

BROADIE K, BAUMGARTNER S & PROKOP A 2011. Extracellular matrix and its receptors in Drosophila neural development. Dev Neurobiol, 71, 1102–30. [PubMed: 21688401]

CHENG J, TURKEL N, HEMATI N, FULLER MT, HUNT AJ & YAMASHITA YM 2008. Centrosome misorientation reduces stem cell division during ageing. Nature, 456, 599–604. [PubMed: 18923395]

CHO JY, CHAK K, ANDREONE BJ, WOOLEY JR & KOLODKIN AL 2012. The extracellular matrix proteoglycan perlecan facilitates transmembrane semaphorin-mediated repulsive guidance. Genes Dev, 26, 2222–35. [PubMed: 23028146]

CHOI HMT, SCHWARZKOPF M, FORNACE ME, ACHARYA A, ARTAVANIS G, STEGMAIER J, CUNHA A & PIERCE NA 2018. Third-generation in situ hybridization chain reaction: multiplexed, quantitative, sensitive, versatile, robust. Development, 145.

DENG WM, SCHNEIDER M, FROCK R, CASTILLEJO-LOPEZ C, GAMAN EA, BAUMGARTNER S & RUOHOLA-BAKER H 2003. Dystroglycan is required for polarizing the epithelial cells and the oocyte in Drosophila. Development, 130, 173–84. [PubMed: 12441301]

FABRIZIO JJ, BOYLE M & DINARDO S 2003. A somatic role for eyes absent (eya) and sine oculis (so) in Drosophila spermatocyte development. Dev Biol, 258, 117–28. [PubMed: 12781687]

FLAHERTY MS, SALIS P, EVANS CJ, EKAS LA, MAROUF A, ZAVADIL J, BANERJEE U & BACH EA 2010. chinmo is a functional effector of the JAK/STAT pathway that regulates eye development, tumor formation, and stem cell self-renewal in Drosophila. Dev Cell, 18, 556–68. [PubMed: 20412771]

FULLER MT 1998. Genetic control of cell proliferation and differentiation in Drosophila spermatogenesis. Semin Cell Dev Biol, 9, 433–44. [PubMed: 9813190]

GORIELY A & WILKIE AO 2012. Paternal age effect mutations and selfish spermatogonial selection: causes and consequences for human disease. Am J Hum Genet, 90, 175–200. [PubMed: 22325359]

GREENSPAN LJ, DE CUEVAS M & MATUNIS E 2015. Genetics of gonadal stem cell renewal. Annu Rev Cell Dev Biol, 31, 291–315. [PubMed: 26355592]

GRMAI L, HARSH S, LU S, KORMAN A, DEB IB & BACH EA 2021. Transcriptomic analysis of feminizing somatic stem cells in the Drosophila testis reveals putative downstream effectors of the transcription factor Chinmo. G3-Genes Genomes Genetics, 11.

GRMAI L, HUDRY B, MIGUEL-ALIAGA I & BACH EA 2018. Chinmo prevents transformer alternative splicing to maintain male sex identity. PLoS Genet, 14, e1007203. [PubMed: 29389999]

HARDY RW, TOKUYASU KT, LINDSLEY DL & GARAVITO M 1979. The germinal proliferation center in the testis of Drosophila melanogaster. J Ultrastruct Res, 69, 180–90. [PubMed: 114676]

HASTINGS IM 1989. Potential germline competition in animals and its evolutionary implications. Genetics, 123, 191–7. [PubMed: 2806882]

ISSIGONIS M, TULINA N, DE CUEVAS M, BRAWLEY C, SANDLER L & MATUNIS E 2009. JAK-STAT signal inhibition regulates competition in the Drosophila testis stem cell niche. Science, 326, 153–6. [PubMed: 19797664]

JIN Z, KIRILLY D, WENG C, KAWASE E, SONG X, SMITH S, SCHWARTZ J & XIE T 2008. Differentiation-defective stem cells outcompete normal stem cells for niche occupancy in the Drosophila ovary. Cell Stem Cell, 2, 39–49. [PubMed: 18371420]

KLAPHOLZ B, HERBERT SL, WELLMANN J, JOHNSON R, PARSONS M & BROWN NH 2015. Alternative mechanisms for talin to mediate integrin function. Curr Biol, 25, 847–57. [PubMed: 25754646]

KLEIN AM & SIMONS BD 2011. Universal patterns of stem cell fate in cycling adult tissues. Development, 138, 3103–11. [PubMed: 21750026]

LEATHERMAN JL & DINARDO S 2010. Germline self-renewal requires cyst stem cells and stat regulates niche adhesion in Drosophila testes. Nat Cell Biol, 12, 806–11. [PubMed: 20622868]

LEE T & LUO L 1999. Mosaic analysis with a repressible cell marker for studies of gene function in neuronal morphogenesis. Neuron, 22, 451–61. [PubMed: 10197526]

MA Q, DE CUEVAS M & MATUNIS EL 2016. Chinmo is sufficient to induce male fate in somatic cells of the adult Drosophila ovary. Development, 143, 754–63. [PubMed: 26811385]

MA Q, WAWERSIK M & MATUNIS EL 2014. The Jak-STAT Target Chinmo Prevents Sex Transformation of Adult Stem Cells in the Drosophila Testis Niche. Dev Cell, 31, 474–86. [PubMed: 25453558]

MCGUIRE SE, MAO Z & DAVIS RL 2004. Spatiotemporal gene expression targeting with the TARGET and gene-switch systems in Drosophila. Sci STKE, 2004, pl6.

NARBONNE-REVEAU K, LANET E, DILLARD C, FOPPOLO S, CHEN CH, PARRINELLO H, RIALLE S, SOKOL NS & MAURANGE C 2016. Neural stem cell-encoded temporal patterning delineates an early window of malignant susceptibility in Drosophila. Elife, 5.

OTTO SP & HASTINGS IM 1998. Mutation and selection within the individual. Genetica, 102–103, 507–24.

RHINER C, DIAZ B, PORTELA M, POYATOS JF, FERNANDEZ-RUIZ I, LOPEZ-GAY JM, GERLITZ O & MORENO E 2009. Persistent competition among stem cells and their daughters in the Drosophila ovary germline niche. Development, 136, 995–1006. [PubMed: 19211674]

SALZMANN V, INABA M, CHENG J & YAMASHITA YM 2013. Lineage tracing quantification reveals symmetric stem cell division in Drosophila male germline stem cells. Cell Mol Bioeng, 6, 441–448. [PubMed: 24465278]

SCHEPERS K, PIETRAS EM, REYNAUD D, FLACH J, BINNEWIES M, GARG T, WAGERS AJ, HSIAO EC & PASSEGUE E 2013. Myeloproliferative neoplasia remodels the endosteal bone marrow niche into a self-reinforcing leukemic niche. Cell Stem Cell, 13, 285–99. [PubMed: 23850243]

SCHNEIDER M, KHALIL AA, POULTON J, CASTILLEJO-LOPEZ C, EGGER-ADAM D, WODARZ A, DENG WM & BAUMGARTNER S 2006. Perlecan and Dystroglycan act at the basal side of the Drosophila follicular epithelium to maintain epithelial organization. Development, 133, 3805–15. [PubMed: 16943280]

SHENG XR & MATUNIS E 2011. Live imaging of the Drosophila spermatogonial stem cell niche reveals novel mechanisms regulating germline stem cell output. Development, 138, 3367–76. [PubMed: 21752931]

SIMONS BD & CLEVERS H 2011. Strategies for homeostatic stem cell self-renewal in adult tissues. Cell, 145, 851–62. [PubMed: 21663791]

SINGH SR, ZHENG Z, WANG H, OH SW, CHEN X & HOU SX 2010. Competitiveness for the niche and mutual dependence of the germline and somatic stem cells in the Drosophila testis are regulated by the JAK/STAT signaling. J Cell Physiol, 223, 500–10. [PubMed: 20143337]

SNIPPERT HJ, SCHEPERS AG, VAN ES JH, SIMONS BD & CLEVERS H 2014. Biased competition between Lgr5 intestinal stem cells driven by oncogenic mutation induces clonal expansion. EMBO Rep, 15, 62–9. [PubMed: 24355609]

SPERLING AS, GIBSON CJ & EBERT BL 2017. The genetics of myelodysplastic syndrome: from clonal haematopoiesis to secondary leukaemia. Nat Rev Cancer, 17, 5–19. [PubMed: 27834397]

STINE RR, GREENSPAN LJ, RAMACHANDRAN KV & MATUNIS EL 2014. Coordinate regulation of stem cell competition by Slit-Robo and JAK-STAT signaling in the Drosophila testis. PLoS Genet, 10, e1004713. [PubMed: 25375180]

TANENTZAPF G, DEVENPORT D, GODT D & BROWN NH 2007. Integrin-dependent anchoring of a stem-cell niche. Nat Cell Biol, 9, 1413–8. [PubMed: 17982446]

VAN DOREN M, WILLIAMSON AL & LEHMANN R 1998. Regulation of zygotic gene expression in Drosophila primordial germ cells. Curr Biol, 8, 243–6. [PubMed: 9501989]

VERMEULEN L, MORRISSEY E, VAN DER HEIJDEN M, NICHOLSON AM, SOTTORIVA A, BUCZACKI S, KEMP R, TAVARE S & WINTON DJ 2013. Defining stem cell dynamics in models of intestinal tumor initiation. Science, 342, 995–8. [PubMed: 24264992]

WALLENFANG MR, NAYAK R & DINARDO S 2006. Dynamics of the male germline stem cell population during aging of Drosophila melanogaster. Aging Cell, 5, 297–304. [PubMed: 16800845]

XU T & RUBIN GM 1993. Analysis of genetic mosaics in developing and adult Drosophila tissues. Development, 117, 1223–37. [PubMed: 8404527]

YAMASHITA YM, JONES DL & FULLER MT 2003. Orientation of asymmetric stem cell division by the APC tumor suppressor and centrosome. Science, 301, 1547–50. [PubMed: 12970569]

ZHU S, LIN S, KAO CF, AWASAKI T, CHIANG AS & LEE T 2006. Gradients of the Drosophila Chinmo BTB-zinc finger protein govern neuronal temporal identity. Cell, 127, 409–22. [PubMed: 17055440]

ZIMMERMAN SG, PETERS NC, ALTARAS AE & BERG CA 2013. Optimized RNA ISH, RNA FISH and protein-RNA double labeling (IF/FISH) in Drosophila ovaries. Nat Protoc, 8, 2158–79. [PubMed: 24113787]

Highlights

- *chinmo*-mutant GSCs secrete ECM proteins to remodel the niche, evicting WT GSCs.
- *chinmo*-mutant GSCs remain in the altered niche by increasing ECM-binding proteins.
- Inheritance of the *chinmo*-mutant allele is biased and occurs in >50% of F1 progeny.
- Aged testes have a remodeled niche caused by declining levels of Chinmo in GSCs.

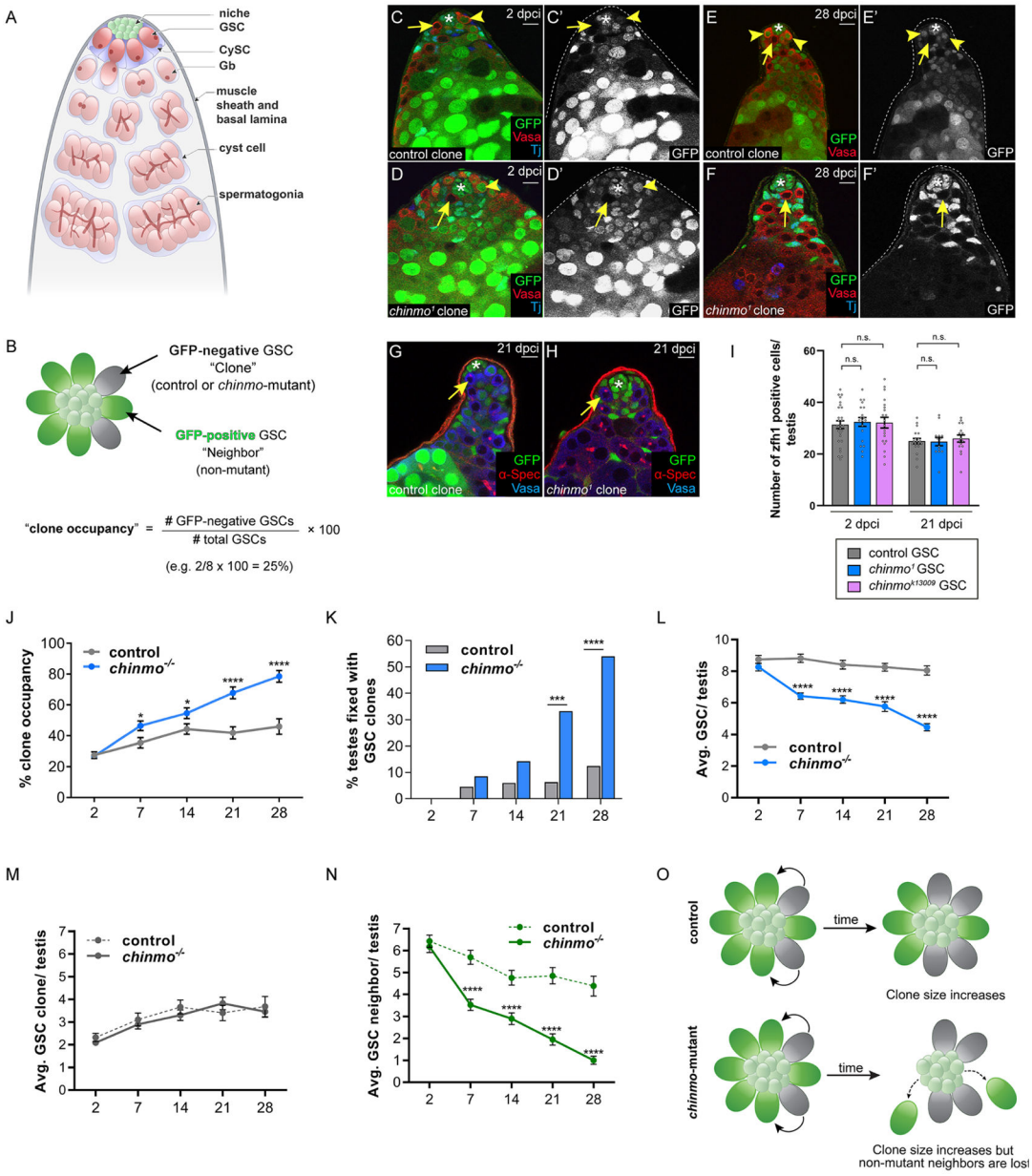

Figure 1: *chinmo*$^{-/-}$ GSCs dominate the niche by evicting non-mutant GSCs.

(A) The adult *Drosophila* testis. A GSC produces a gonialblast (Gb), which undergoes transita-mplifying divisions to produce spermatogonia that differentiate into sperm. CySCs divide to produce cyst cells, two of which envelope a Gb and its descendants.

(B) The clone occupancy assay. In a WT testis, 8 GSCs surround the niche. GSC clones (either control or *chinmo*$^{-/-}$) lack GFP. The other GSCs (labeled "neighbors") are not mutant and express GFP. Clone occupancy is measured by dividing the number of GSC clones by the total number of GSCs in that testis.

(C-F) Confocal images of testes with control (C,E, arrows) or *chinmo*$^{-/-}$ (D,F, arrows) GSC clones at 2 (C,D) or 28 (E,F) dpci. Clones lack GFP. Vasa (red) marks germ cells. Tj

(blue) marks the nuclei of CySCs and early cyst cells. Arrowheads mark non-mutant GSC neighbors.

(G-H) Confocal images of testes with control (G, arrow) or *chinmo*$^{-/-}$ (H, arrow) clones at 21 dpci stained with αSpectrin (red) to mark the fusome. Clones lack GFP. Vasa (blue).

(I) Graph showing the number of Zfh1-positive CySCs in testes with control (gray), *chinmo*^{1} (blue) and *chinmo*^{k13009} GSC clones (purple) at 2 and 28 dpci.

(J) Graph showing clone occupancy of control (gray) and *chinmo*$^{-/-}$ (blue) GSC clones at 2, 7, 14, 21, 28 dpci.

(K) Graph showing percent monoclonal testes within the GSC lineage at 2, 7, 12, 21 and 28 dpci when control (gray) or *chinmo*$^{-/-}$ (blue) GSC clones are present.

(L) Graph showing the average total number of GSCs in testes with control (gray) or *chinmo*$^{-/-}$ GSC clones (blue) at 2, 7, 14, 21 and 28 dpci.

(M) Graph showing the average number of control (dashed line) or *chinmo*$^{-/-}$ (solid line) GSC clones at 2, 7, 14, 21 and 28 dpci.

(N) Graph showing non-mutant GSC neighbors in testes with control (dashed line) or *chinmo*$^{-/-}$ (solid line) GSC clones at 2, 7, 14, 21 and 28 dpci.

(O) Model. Control GSC clones (gray cells, upper panel) and *chinmo*$^{-/-}$ GSC clones (gray cells, lower panel) are induced at the same low frequency. Over time, both types of clones expanded to a similar extent (gray cells). *chinmo*$^{-/-}$ clones cause the loss of non-mutant neighbor GSCs (green cells, lower panel) and this does not occur to the non-mutant neighbors (green cells, upper panel) of control GSC clones.

In C-F, G,H, an asterisk marks the niche.

Scale bar = 10 μM

In I,J,L,M,N, error bars represent SEM.

n.s. = not significant; * $P \leq 0.05$; *** $P \leq 0.001$; **** $P \leq 0.0001$ as assessed by Student's t-test (I,J,LM,N) or by χ^2 test (K).

See also Table S1, Fig. S1.

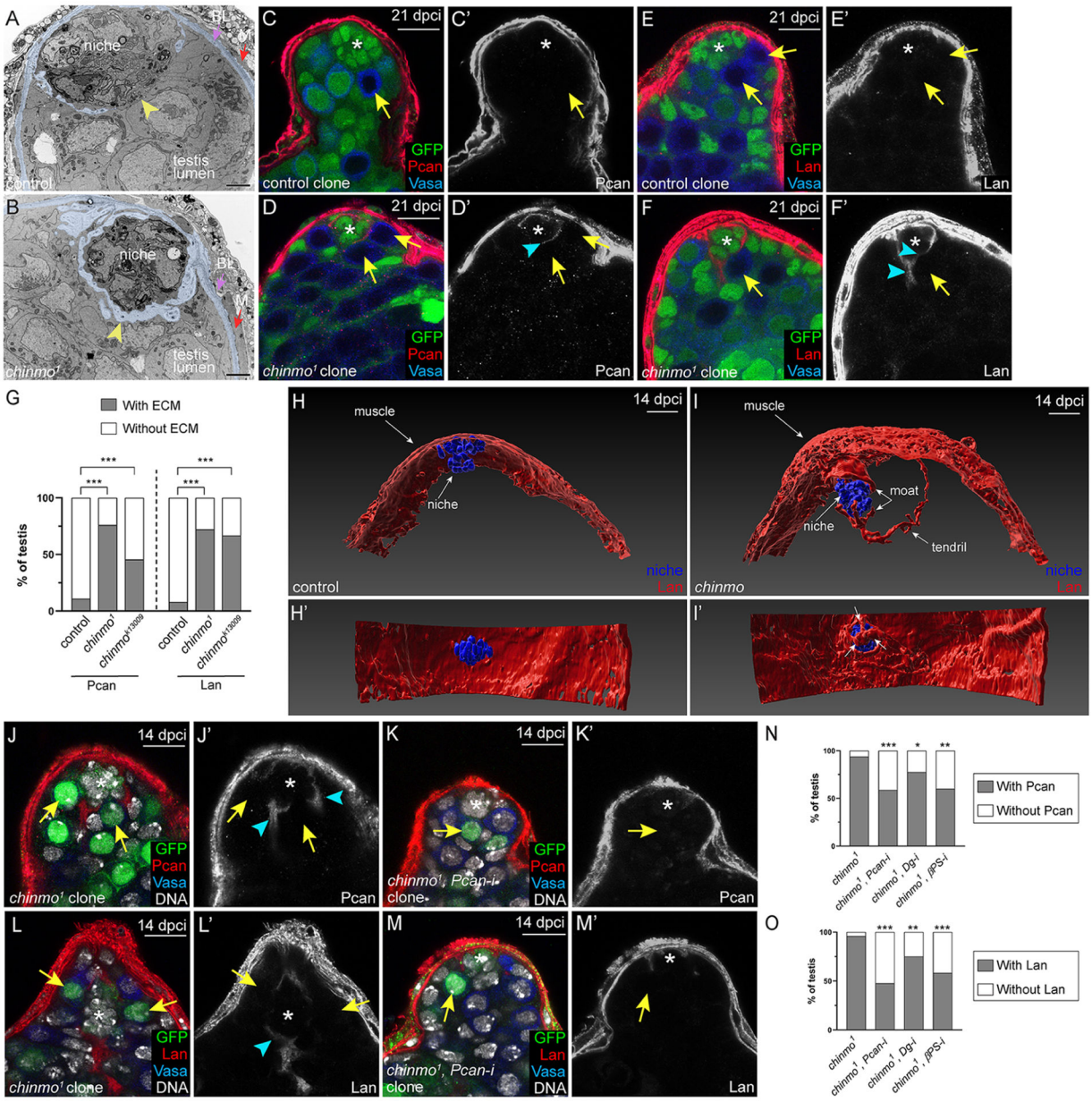

Figure 2: *chinmo*$^{-/-}$ GSCs create a "moat" around the niche by secreting Pcan

(A,B) TEMs of testes with control (A) or *chinmo*^{1} (B) GSC clones at 28 dpci. The micrographs are pseudocolored to show ECM-like material (light blue) in the muscle basal lamina ("BL", purple arrowhead in A,B) or in the testis lumen (yellow arrowhead, B). Yellow arrowheads indicate GSC-niche interface. Magnification 5,600x. Scale bar is 2 μM.

(C-F) Pcan (C,D, red) and Lan (E,F, red) in testes with control (C,E arrows) *chinmo*$^{-/-}$ GSC (D,F, arrow) clones at 21 dpci. Arrowhead (D',F') indicates ectopic ECM.

(G) Graph quantifying the percentage testes with (gray portion of bar) or without (white portion of bar) ECM proteins Pcan or Lan surrounding the niche when control, *chinmo*^{1} or *chinmo*^{k13009} clones are present.

(H,I) Imaris-generated view of a testis with control (H) or *chinmo*$^{-/-}$ (I) GSC clones (not shown) at 14 dpci. Niche cells (blue) are visible as a ball, and some niche cells adhere to Lan (red) present in the muscle (H,I). In I, some niche cells are partially obscured by a distended "hat" of Lan (red, upper arrow labeled "moat") that is contiguous with Lan in the muscle. In I, there is ectopic Lan in the testis lumen, which form three "claws" on distal niche cells (lower arrow labeled "moat"). A "tendril" of ectopic Lan extends to the right. In H',I', the testis is rotated 90°. All niche cells are visible in H', but in I' several niche cells are covered by Lan (arrows).

(J-M) Expression of Pcan (red in J,K) and Lan (red in L,M) around the niche when *chinmo*$^{-/-}$ GSC clones (J,L) or *chinmo*$^{-/-}$ clones depleted for Pcan (K,M) are present. Arrowheads indicate ectopic ECM.

(N-O) Graph quantifying the percentage of testes with (gray portion of bar) or without (white portion of bar) Pcan (N) or Lan (O) in the moat when *chinmo*$^{-/-}$ clones (first bars), *chinmo*$^{-/-}$ clones depleted for Pcan (second bars), for Dg (third bars) or for βPS (fourth bars) are present. In A-F, clones lack GFP. In H-M, clones express GFP. In C-F, J-M, Vasa is blue and an asterisk marks the niche.

Scale bar = 10 μM

* $P \leq 0.05$; ** $P \leq 0.01$; *** $P \leq 0.001$ as assessed by χ^2 test. See also Figs. S1, S2, S4, S7.

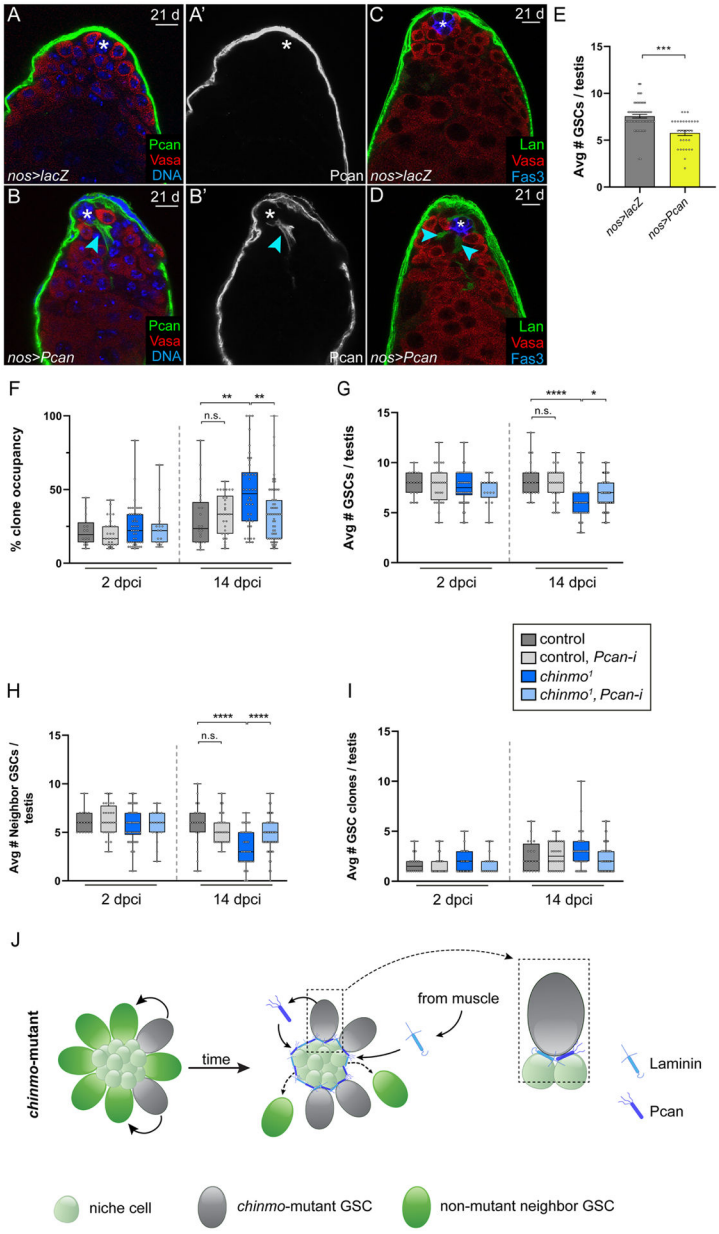

Figure 3: *chinmo*$^{-/-}$ GSCs require Pcan to evict non-mutant neighbors

(A,D) Confocal images of *nos>lacZ* (A,C) or *nos>Pcan* (B,D) testes in which Pcan was mis-expressed in all GSCs for 21 days. Arrowheads (B,B',D) indicate ectopic ECM. Pcan (green, A,B); Lan (green, C,D); Vasa (red) and DNA (ToPro, blue A,B); Fas3 (blue, C,D). (E) Graph showing average number of GSCs in *nos>lacZ* (gray) or *nos>Pcan* (yellow) testes. (F-I) Box and whisker plots showing clone occupancy (F), average total number of GSCs (G), average number of non-mutant GSC neighbors (H); average number of clones (I) in testis with control GSC clones (dark gray bars), with control GSC clones depleted for Pcan (light gray bars), with *chinmo*$^{-/-}$ GSC clones (dark blue bars) or *chinmo*$^{-/-}$ GSC clones depleted for Pcan (light blue bars) at 2 and 14 dpci.

(J) Model: *chinmo*$^{-/-}$ GSC clones (gray cells) secrete Pcan (dark blue symbol), which seeds the moat. Lan (light blue symbol) is recruited from the muscle BL. Boxed area at right illustrates a *chinmo*$^{-/-}$ GSC clone in contact with the moat. By contrast, non-mutant neighbor GSCs (green stem cells in middle cartoon) are lost from the niche. The smaller, light green cells are niche cells.

Scale bar = 10 μM

In F-I, error bars represent SEM.

n.s. = not significant; * $P \leq 0.05$; ** $P \leq 0.01$; *** $P \leq 0.001$; **** $P \leq 0.0001$, as assessed by Student's t-test.

See also Table S1, Figs. S1, S3, S7.

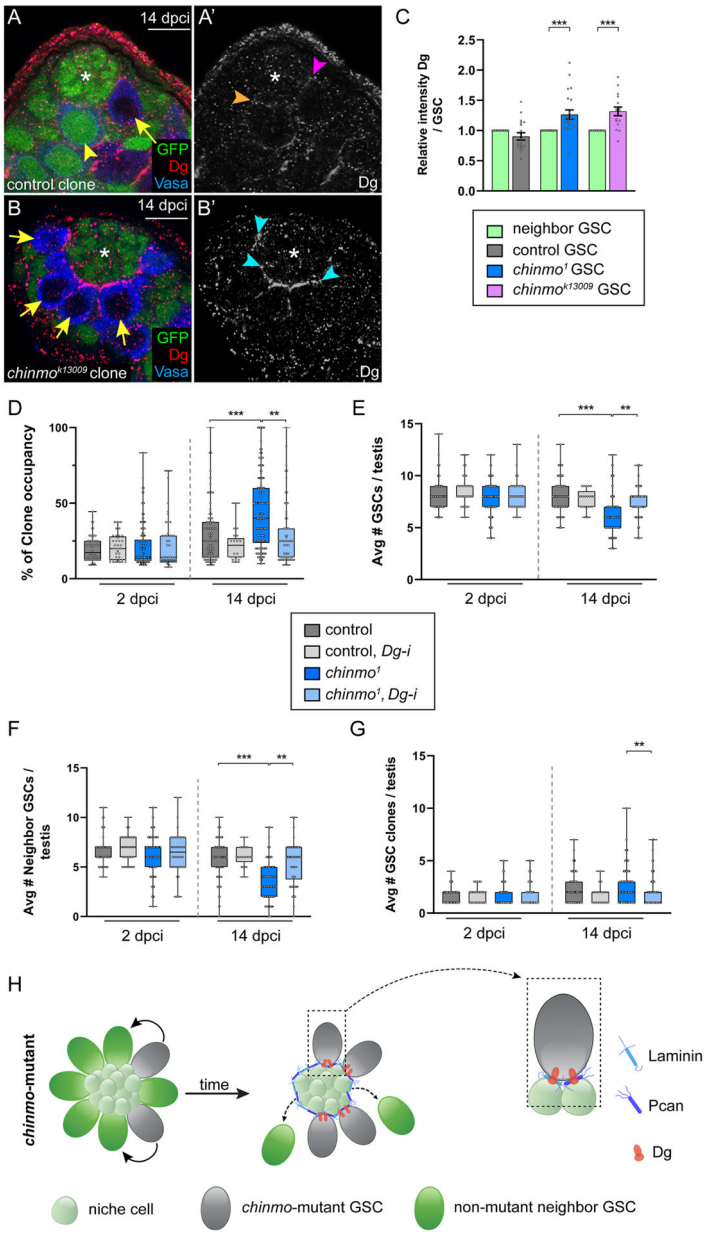

Figure 4: *chinmo*$^{-/-}$ GSCs require Dg to remain in the altered niche

(A,B) Confocal images of Dg (red) in testes harboring control (A, arrow) or *chinmo*^{k13009}-mutant GSC clones (B, arrows) at 14 dpci. Orange arrowhead (A'), magenta arrowhead (A') and blue arrowheads (B') indicate Dg at the GSC-niche in a non-mutant GSC neighbor, a control clone and a *chinmo*$^{-/-}$ GSC, respectively. Clones lack GFP. Neighbors (yellow arrowhead) express GFP. Vasa (blue).

(C) Graph of relative Dg expression at the GSC-niche interface in control, *chinmo*^{1} or *chinmo*^{k13009} GSC clones relative to that of neighbor GSCs in the same testis.

(D-G) Box and whisker plots showing clone occupancy (D), average total number of GSCs (E), average number of non-mutant GSC neighbors (F), and average numbers of GSC clones (G) in testes with control GSC clones (dark gray bars), with control GSC clones depleted for

Dg (light gray bars), with *chinmo*$^{-/-}$ GSC clones (dark blue bars) or *chinmo*$^{-/-}$ GSC clones depleted for Dg (light blue bars) at 2 and 14 dpci.

(H) Model: *chinmo*$^{-/-}$ GSC clones (gray cells) have increased Dg (orange symbol) at the GSC-niche interface, allowing them to remain in the resculpted niche. Boxed area at right illustrates a *chinmo*$^{-/-}$ GSC clone remaining in contact with the moat through increased localized Dg expression. Non-mutant neighbor GSCs do not have increased Dg at the GSC-niche interface and cannot remain long-term in the niche.

Scale bar = 10 μM

In D-G, error bars represent SEM.

* $P \leq 0.05$; ** $P \leq 0.01$; *** $P \leq 0.001$; **** $P \leq 0.0001$, as assessed by Student's t-test.

See also Table S1, Figs. S1, S4, S5, S6.

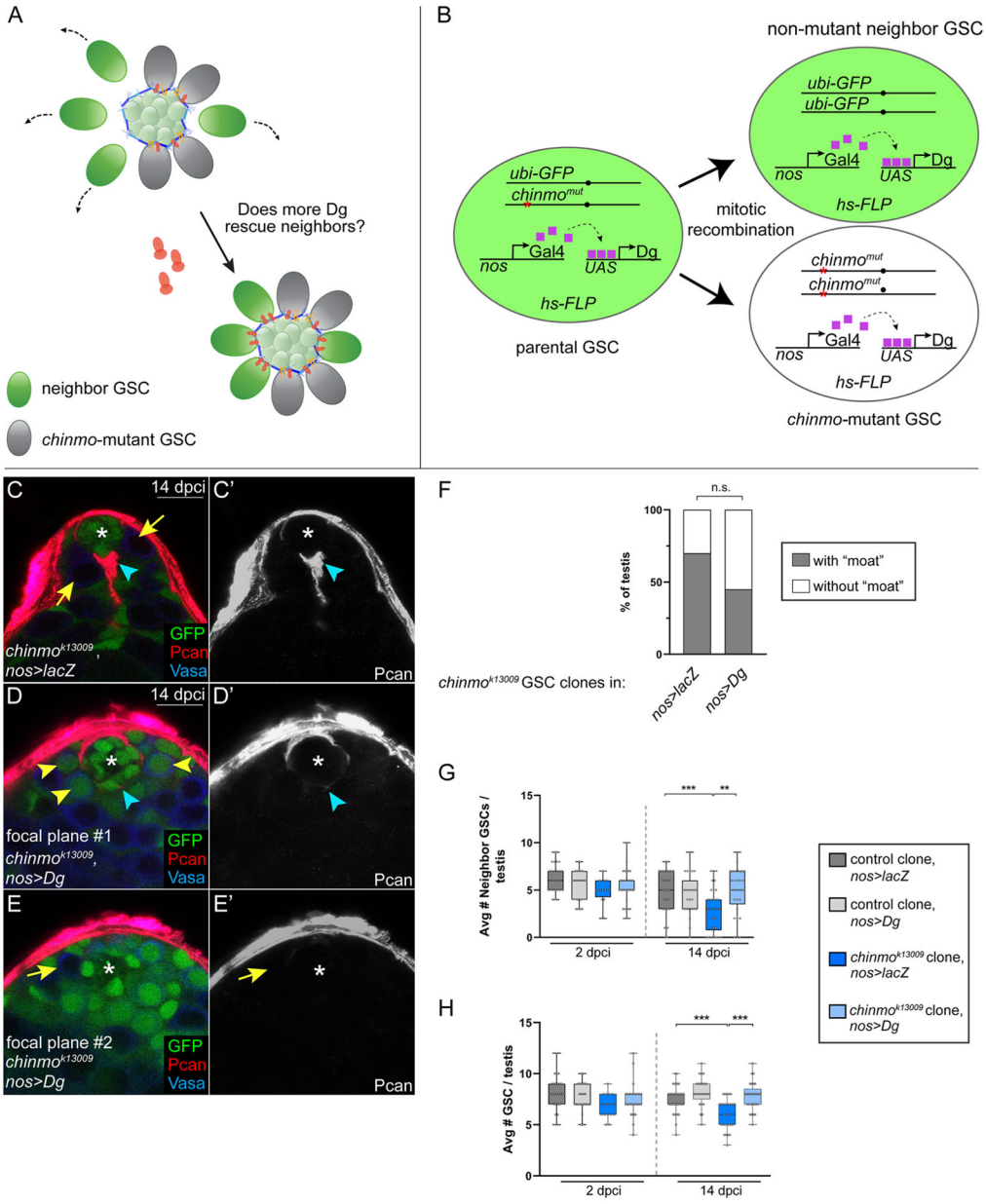

Figure 5: Neighbors are rescued from competition when provide with ectopic Dg

(A) Model: If non-mutant neighbor GSCs (green) are provided with increased Dg (dark orange), they should be able to remain in the niche despite the induction of *chinmo*$^{-/-}$ GSC clones (gray) and the formation of the moat (Pan, Lan, blue symbols). Yellow symbols represent integrins.

(B) In the "neighbor rescue" assay, *chinmo*$^{-/-}$ clones (abbreviated *chinmo*^{mut}) were generated in a background where all GSCs express *UAS-Dg* driven by the GSC driver *nos-Gal4*. We scored the number of non-mutant neighbors at 2 and 14 dpci (see G), average number of GSCs (see H) and presence a moat (see C,D,F).

(C-E) Pcan (red) in testes containing *chinmo*^{k13009} GSC clones in *nos>lacZ* (C) or *nos>Dg* (D). The *chinmo* clone is not visible in D (“focal plan #1”) but is visible in E (arrow, “focal plane #2”). Clones lack GFP. Pcan (red). Vasa (blue).

(F) Graph showing percentage of testes with a “moat” when *chinmo*^{k13009} GSC clones are generated in a *nos>lacZ* or *nos>Dg* background.

(G, H) Box and whisker plots showing average number of non-mutant GSC neighbors (G) or average number of GSCs (H) in testis with control GSC clones in *nos>lacZ* (dark gray bars), control GSC clones in *nos>Dg* (light gray bars), *chinmo*^{k13009} GSC clones in *nos>lacZ* (dark blue bars), or *chinmo*^{k13009} GSC clones in *nos>Dg* (light blue bars) at 2 and 14 dpci. Scale bar = 10 μM

In G,H, error bars represent SEM.

n.s. = not significant; ** P ≤ 0.01; *** P ≤ 0.001 as assessed by Student’s t-test (G,H) and by χ^2 test (F).

See also Table S2.

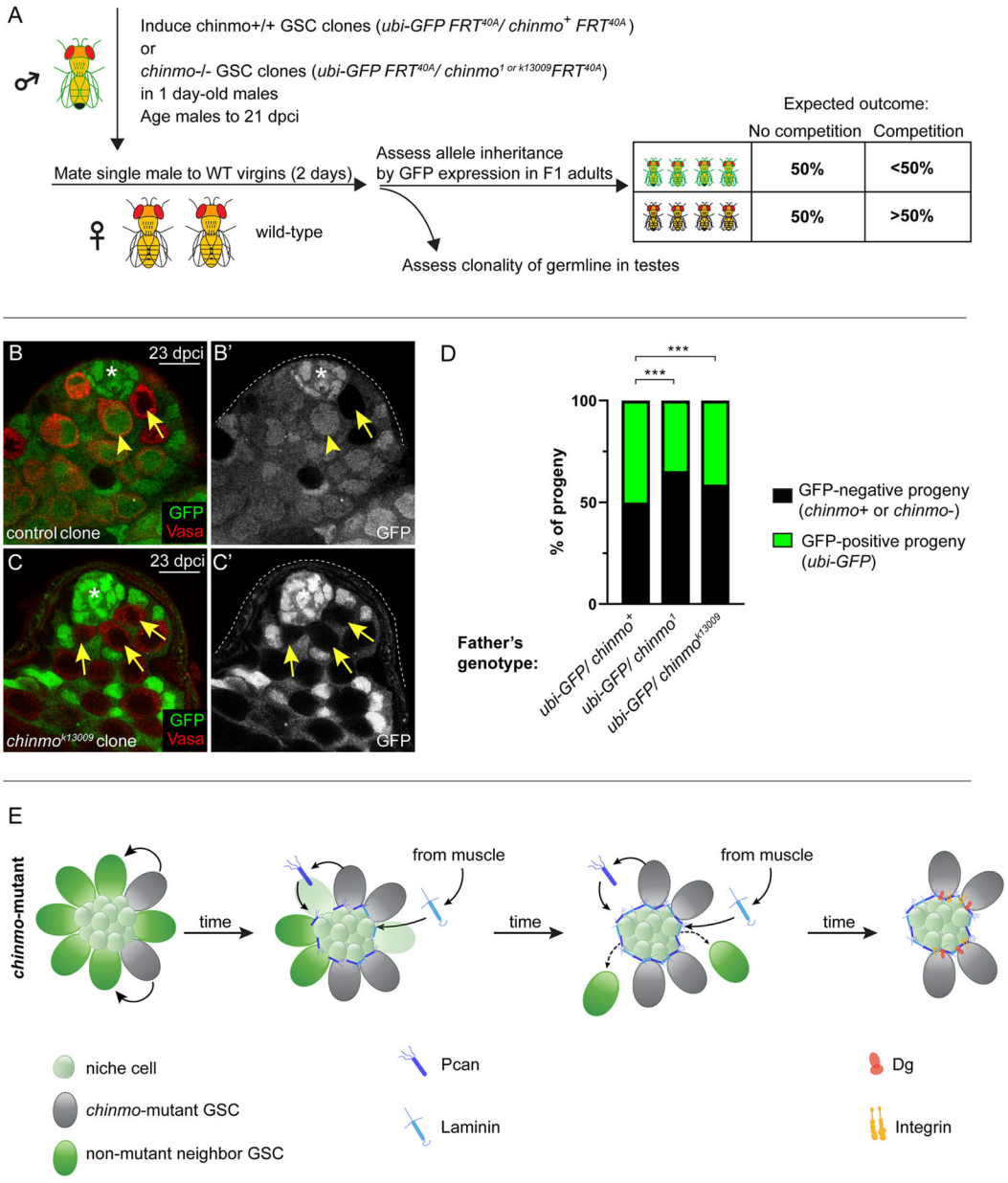

Figure 6: GSC competition causes biased inheritance

(A) Schematic of the "inheritance assay" - see STAR Methods for details. Box shows expected outcomes.

(B,C) Confocal images of a testis with a control (B,B', arrow) or a *chinmo*^{k13009} GSC clone (C,C', arrows) at 23 dpci. Non-mutant neighbor GSCs are marked by an arrowhead. The only GFP-positive cells in C are somatic support cells. Clones lack GFP. Vasa is red.

(D) Graph showing inheritance of the *chinmo* chromosome (*chinmo*$^{+}$, *chinmo*^{1} or *chinmo*^{k13009} allele) (in black) or the *ubi-GFP* chromosome (in green).

(E) Model. *chinmo*$^{-/-}$ GSC clones (gray) secrete Pcan (dark blue), which causes the moat. Lan (light blue) is recruited to the moat from the muscle BL. *chinmo*$^{-/-}$ GSC clones increase

Dg (orange) and βPS integrin (yellow) at the GSC-niche interface, allowing them to remain in the resculpted niche but non-mutant neighbor GSCs (green cells) do not and differentiate. Scale bar = 10 μM

*** $P \leq 0.001$ as assessed by χ^2 test (D).

See also Table S3.

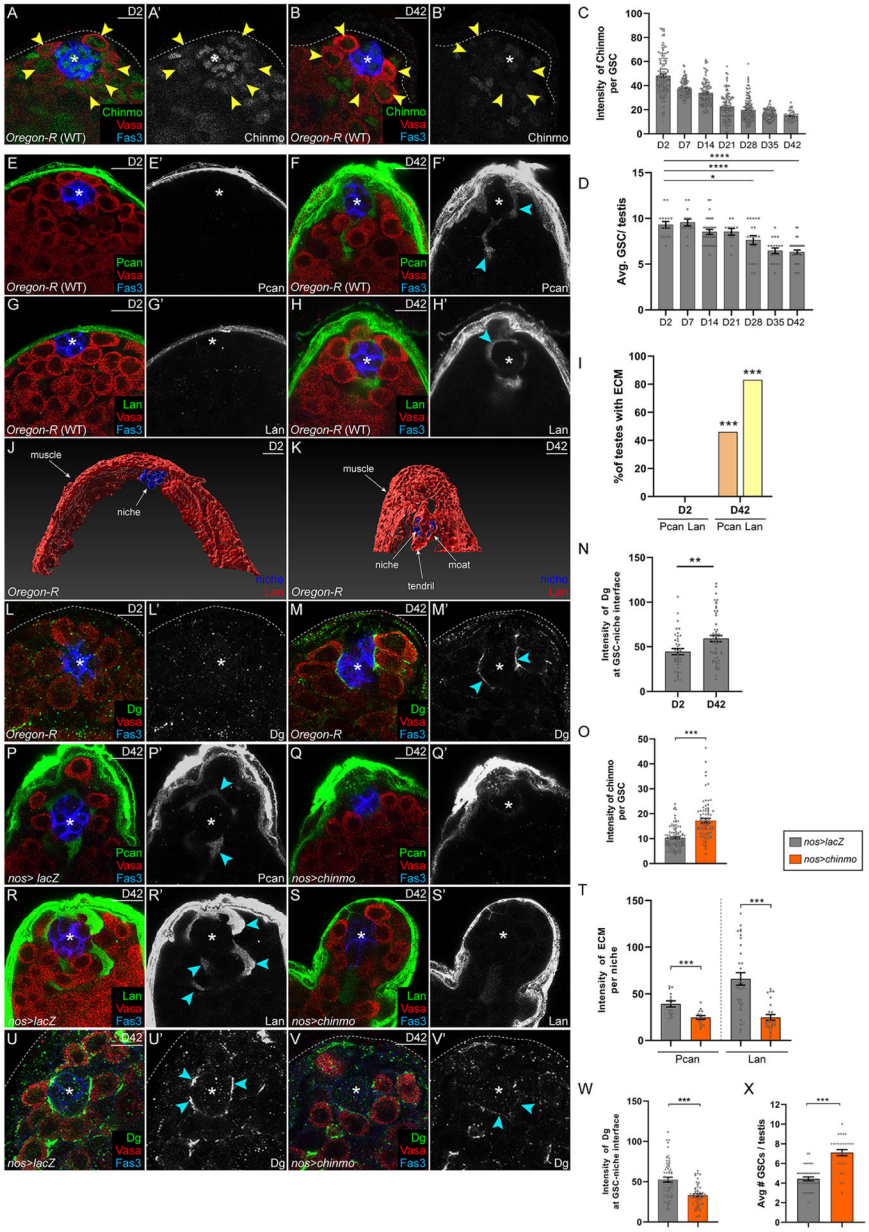

Figure 7: Age-related phenotypes of the testis stem cell niche are caused by declining Chinmo levels in GSCs

(A-D) Confocal images of young (2-day-old) (A) or aged (42-day-old) (B) WT testes. Chinmo (green). Arrowheads indicate GSCs in A,B. (C,D) Graphs showing Chinmo levels in GSCs (C) and average number of GSCs/testis (D) during aging.

(E-H) Confocal image of Pcan (green in E,F) and Lan (green in G,H) in young (E,G) and aged testes (F,H). (I) Graph showing percentage of testis with Pcan (orange) or Lan (yellow) surrounding the niche.

(J,K) Imaris-generated views of young (J) and aged (K) testes. Niche cells (blue) are visible as a ball (J,K). In a young testis, some niche cells interact with Lan (red) present in muscle BL (J). In an aged testis, some niche cells are partially obscured by ectopic Lan (red) in the testis lumen (K).

(L-N) Confocal image of young (L) and aged (M) testis stained with Dg (green). (N) Graph showing relative Dg levels at the GSC-niche interface in young or old testes.
(O) Graph showing Chinmo intensity in GSCs in *nos>lacZ* (gray) or *nos>chinmo* (orange).
(P-T) Confocal images of aged *nos>lacZ* (P,R) and aged *nos>chinmo* (Q,S) testes stained for Pcan (green in P,Q) or Lan (green in R,S). (T) Graph showing ECM intensity in aged *nos>lacZ* (gray) or aged *nos>chinmo* (orange) testes.
(U-X) Confocal images of aged *nos>lacZ* (U) or aged *nos>chinmo* (V) testes stained with Dg (green). Arrowheads indicate Dg at GSC-niche interface. (W) Graph of Dg intensity at the GSC-niche interface in aged *nos>lacZ* (gray) or in aged *nos>chinmo* (orange) testes.
(X) Graph showing number of GSCs in aged *nos>lacZ* (gray) or in aged *nos>chinmo* (orange) testes.
In A,B,E-H,L,M,P-S,U,V, Vasa is red and Fas3 is blue.
Scale bar = 10 μM
In C,D,N,O,T,W,X, error bars represent SEM.
* $P \leq 0.05$; ** $P \leq 0.01$; *** $P \leq 0.001$; **** $P \leq 0.0001$ as assessed by Student's t-test (C,D,N,O,T,W,X) and by χ^2 test (I).
See also Table S1.

Key Resource Table

REAGENT or RESOURCE	SOURCE	IDENTIFIER
Antibodies		
Rabbit polyclonal anti-GFP (1:1000)	Invitrogen	Cat# A6455
Goat polyclonal anti-Vasa (1:200)	Santa Cruz	Cat# sc26877; RPID: AB_793877
Rabbit polyclonal anti-Zfh1 (1:200)	K. White (University of Chicago, USA)	N/A
Guinea pig polyclonal anti-Traffic jam (Tj) (1:1000)	D. Godt (University of Toronto, Canada)	N/A
Rabbit polyclonal anti-Pcan (1:1000)	Baumgartner lab	N/A
Chicken polyclonal anti-Vasa (1:200)	P. Rangan (SUNY, Albany, USA)	N/A
Rat anti-Chinmo (1:200)	N. Sokol (Indiana University, USA)	N/A
Chicken polyclonal anti-GFP (1:1000)	Abcam	Cat# ab13970 RRID:AB_300798
Guinea pig anti-Lan (1:1000)	T. Volk (Weizmann Institute, Israel)	N/A
Rabbit polyclonal anti-Dg (1:500)	Baumgartner lab	N/A
Mouse monoclonal anti-Talin carboxy terminus 534 amino acids (1:20)	Developmental Studies Hybridoma Bank (DSHB)	Cat# Talin E16B, RRID:AB_10683995
Mouse monoclonal anti-Talin carboxy terminus 534 amino acids (1:20)	DSHB	Cat# Talin A22A, RRID:AB_10660289
Mouse monoclonal anti-β-galactosidase (1:50)	DSHB	Cat# 40-1a RRID:AB_528100
Mouse monoclonal anti-βPS integrin (1:20)	DSHB	Cat# cf.6g11 RRID:AB_528310
Guinea pig anti-Myc (1:50)	G. Morata (CSIC-UAM, Spain)	N/A
Rabbit anti-cleaved Dcp-1 (1:500)	Cell Signaling	Cat# 9578 RRID:AB_2721060
Mouse monoclonal anti-γ-tubulin (1:1000)	Sigma-Aldrich	Cat# T6557 RRID:AB_477584
Rabbit polyclonal anti-phospho-Mad (1:1250)	E. Laufer (Columbia University, USA)	N/A
Rabbit polyclonal anti-pSTAT (1:50)	Bach lab	N/A
Rat monoclonal anti-E-Cad (1:5)	DSHB	Cat# DCAD2 RRID:AB_528120
Rabbit polyclonal anti-ColIV (1:500)	B. Hudson (Vanderbilt University, USA)	N/A
Rabbit polyclonal anti-Testican (1:500)	Baumgartner lab	N/A
Rabbit polyclonal antiNidogen (1:400)	Baumgartner lab	N/A
Rabbit polyclonal anti-Sparc (1:200)	M. Ringuette (University of Toronto, Canada)	N/A
Mouse monoclonal anti-αPS1 integrin (1:100)	DSHB	Cat# dk.1a4 RRID:AB_528303
Mouse monoclonal anti-αPS2 integrin (1:100)	DSHB	Cat# cf.2c7 RRID:AB_528304
Rabbit polyclonal anti-αPS3 integrin (1:100)	S. Hayashi (RIKEN Center for Developmental Biology, Japan)	N/A
Rabbit polyclonal anti-αPS4 integrin (1:100)	M. Crozatier (Université de Toulouse, France)	N/A
Mouse monoclonal anti-βν integrin (1:200)	Y. Nakanishi (Kanazawa University, Japan)	N/A
Mouse monoclonal anti-Drosophila α-Spectrin (1:20)	DSHB	Cat# 3A9 RRID:AB_528473
Cy3-AffiniPure Donkey Anti-Mouse IgG (1:400)	Jackson ImmunoResearch Labs	Cat# 715-165-150 RRID:AB_2340813

REAGENT or RESOURCE	SOURCE	IDENTIFIER
Alexa Fluor 488-AffiniPure Donkey Anti-Rabbit IgG (H+L) (1:400)	Jackson ImmunoResearch Labs	Cat# 711-545-152 RRID:AB_2313584
Cy3-AffiniPure Donkey Anti-Rabbit IgG (H+L) (1:400)	Jackson ImmunoResearch Labs	Cat# 711-165-152 RRID:AB_2307443
Cy5-AffiniPure Donkey Anti-Rabbit IgG (H+L) (1:400)	Jackson ImmunoResearch Labs	Cat# 711-175-152 RRID:AB_2340607
Alexa Fluor 488-AffiniPure Donkey Anti-Rat IgG (H+L) (1:400)	Jackson ImmunoResearch Labs	Cat# 712-545-150 RRID:AB_2340683
Cy3-AffiniPure Donkey Anti-Rat IgG (H+L) (1:400)	Jackson ImmunoResearch Labs	Cat# 712-165-150, RRID:AB_2340666
Cy5-AffiniPure Donkey Anti-Rat IgG (H+L) (1:400)	Jackson ImmunoResearch Labs	Cat# 712-175-150, RRID:AB_2340671
Alexa Fluor 488 AffiniPure Donkey Anti-Chicken IgY (IgG) (H+L) (1:400)	Jackson ImmunoResearch Labs	Cat# 703-545-155, RRID:AB_2340375
Cy3-AffiniPure Donkey Anti-Chicken IgY (IgG) (H+L) (1:400)	Jackson ImmunoResearch Labs	Cat# 703-165-155, RRID:AB_2340363
Cy5-AffiniPure Donkey Anti-Chicken IgY (IgG) (H+L) (1:400)	Jackson ImmunoResearch Labs	Cat# 703-175-155, RRID:AB_2340365
Cy3-AffiniPure Donkey Anti-Guinea Pig IgG (1:400)	Jackson ImmunoResearch Labs	Cat# 706-165-148, RRID:AB_2340460
Cy5-AffiniPure Donkey Anti-Guinea Pig IgG (H+L) (1:400)	Jackson ImmunoResearch Labs	Cat# 706-175-148, RRID:AB_2340462
Cy3-AffiniPure Donkey Anti-Goat IgG (H+L) (1:400)	Jackson ImmunoResearch Labs	Cat# 705-165-003, RRID:AB_2340411
Alexa Fluor 647 AffiniPure Donkey Anti-Goat IgG (H+L) (1:400)	Jackson ImmunoResearch Labs	Cat# 705-605-003, RRID:AB_2340436
Chemicals, peptides, and recombinant proteins		
VECTASHIELD Mounting Medium with DAPI	Vector Laboratories	Cat# H-1200, RRID:AB_2336790
VECTASHIELD Mounting	Vector Laboratories	Cat# H-1000, RRID:AB_2336789
Paraformaldehyde, 16% w/v aq. soln., methanol free (PFA)	Thermo Fisher Scientific	Cat# 43368-9L
Heparin	Sigma-Aldrich	Cat# H4784
tRNA	Roche	Cat# 10109495001
Protector RNase Inhibitor	Roche	Cat# 3335399001
20 × Saline Sodium Citrate (SSC)	Thermo Fisher	Cat# 15557-044
Proteinase K	Thermo Fisher Scientific	Cat# EO0491
Glycine	Thermo Fisher Scientific	Cat# BP381-500
Diethyl pyrocarbonate (DEPC)	MilliporeSigma	Cat# D5758
Click-iT EdU Imaging Kits	Thermo Fisher Scientific	Cat# C10340
Molasses	Labscientific	Cat# FLY-8008-16
Agar	Mooragar	Cat# 41004
Cornmeal	LabScientific	Cat# FLY-8010-20
Yeast	LabScientific	Cat# FLY-8040-20F
Tegosept	Sigma	Cat# H3647-1KG
Reagent alcohol	Fisher	Cat# A962P4
Propionic acid	Fisher	Cat# A258500
Experimental Models: Organisms/Strains		
D. melanogaster; *y, w, hs-flp^{122}/Y; ubi-GFP, FRT^{40A}*	Bach lab	N/A

REAGENT or RESOURCE	SOURCE	IDENTIFIER
D. melanogaster; *w; chinmo^{1},UAS-mCD8-GFP, FRT^{40A}/CyO*	T. Lee (Janelia Research Camp, USA)	N/A
D. melanogaster; *w; P[ry[+t7.2]=neoFRT]^{40A}*;	Bach lab	N/A
D. melanogaster; *y, w, hs-flp^{122}, tub-Gal4, UAS-nls-GFP/Y; tub-Gal80, FRT^{40A}/CyO*	Bach lab	N/A
D. melanogaster; y^{1} v1; P[TRiP.GL01153]attP2 (*Pcan-i* #1)	BDSC	RRID:BDSC_42783
D. melanogaster; *y^{1} v^{1}; P[TRiP.JF03376]attP2* (*Pcan-i* #2)	BDSC	RRID:BDSC_29440
D. melanogaster; *y, w; P[w+, nos-GAL4 VP16]* on II	Bach lab	N/A
D. melanogaster; *w^{1118}; P[w[+mC]=UAS-lacZ.NZ]J312* Insertion on III	BDSC	RRID:BDSC_3956
D. melanogaster; *w; UAS-PcanRG* Insertion on III	A. Kolodkin (Johns Hopkins School of Medicine, USA)	N/A
D. melanogaster; *y^{1} sc* v^{1} sev^{21};P[TRiP.HMS01240]attP 2*(*Dg-i*)	BDSC	RRID:BDSC_34895
D. melanogaster; *w; P[lacW]chinmo^{k13009}, FRT^{40A}/CyO*	Kyoto Stock Center	RRID:DGGR_111100
D. melanogaster; *y, w, βPS-GFP*	N. Brown (University of Cambridge, UK)	N/A
D. melanogaster; *y^{1} v^{1}; P[TRiP.HMS00036]attP2/TM3, Sb^{1}* (*chinmo-i*)	BDSC	RRID:BDSC_33638
D. melanogaster; *y^{1} v^{1}; P[TRiP.HMS00043]attP2* (*βPS-i* #1)	BDSC	RRID:BDSC_33642
D. melanogaster; *y^{1} v^{1}; P[TRiP.JF02819]attP2* (*βPS-i* #2)	BDSC	RRID:BDSC_27735
D. melanogaster; *w; UAS-Dg* Insertion on III	W. Deng (Tulane University, USA)	N/A
D. melanogaster; *y^{1} sc* v^{1} sev^{21}; P[TRiP.HMS00799]attP2* (*talin-i*)	BDSC	RRID:BDSC_32999
D. melanogaster; *y^{1} sc* v^{1} sev^{21};P[TRiP.HMS02451]attP 2*(*Lan-i*)	BDSC	RRID:BDSC_42616
D.melanogaster; w; P[Mef2-Gal4.247]3*	BDSC	RRID:BDSC_50742
D. melanogaster; *y^{1} sc* v^{1} sev^{21}; P[TRiP.HMS00799]attP2* (*talin-i*)	BDSC	BDSC: 32999 FlyBase: FBst0032999
D. melanogaster; *w; +; UAS-5'UTR-chinmo-3'UTR*	T. Lee (Janelia Research Camp, USA)	N/A
D. melanogaster; w; P[UAS-mCherry.scramble.sponge]att P40; P[UAS mCherry.scramble.sponge]att P2* (*control-i*)	BDSC	RRID:BDSC_61507
D. melanogaster; w^{1118}; P[GD7744]v24549 (*Pcan-i* on II)	VDRC	RRID:SCR_24549
D. melanogaster; w; P[GawB]NP1624/CyO;* (*tj-Gal4)*	Bach lab	RRID:DGGR_104055
D. melanogaster; w ^{1118} ; P[w+mC=UAS-Dcr-2.D]10 (UAS-Dcr-2)	Bach lab	RRID:BDSC_24651
D.melanogaster; w; P[tubP-Gal80ts]2/TM2*	BDSC	RRID:BDSC_7071
Oligonucleotide		
HCR probe of *Pcan*	Molecular Instruments, Inc.	LOT: PRJ993
HCR probe of *Dg*	Molecular Instruments, Inc.	LOT: PRJ994
HCR probe of *βPS*	Molecular Instruments, Inc.	LOT: PRJ995
Software and algorithms		
ImageJ/Fiji	Fiji	http://fiji.sc/
Photoshop/Illustrator	Adobe	https://www.adobe.com/products/
Prism	GraphPad	https://www.graphpad.com
ZEN	Zeiss	https://www.zeiss.com/microscopy/us/products/microscopesoftware/zen.html

REAGENT or RESOURCE	SOURCE	IDENTIFIER
Excel	Microsoft	https://products.office.com/en-us/excel
Imaris	Oxford Instruments	https://imaris.oxinst.com/